iScience

Article

LAMP2A regulates endosomal protein composition and membrane identity in exosome biogenesis

Graphical abstract

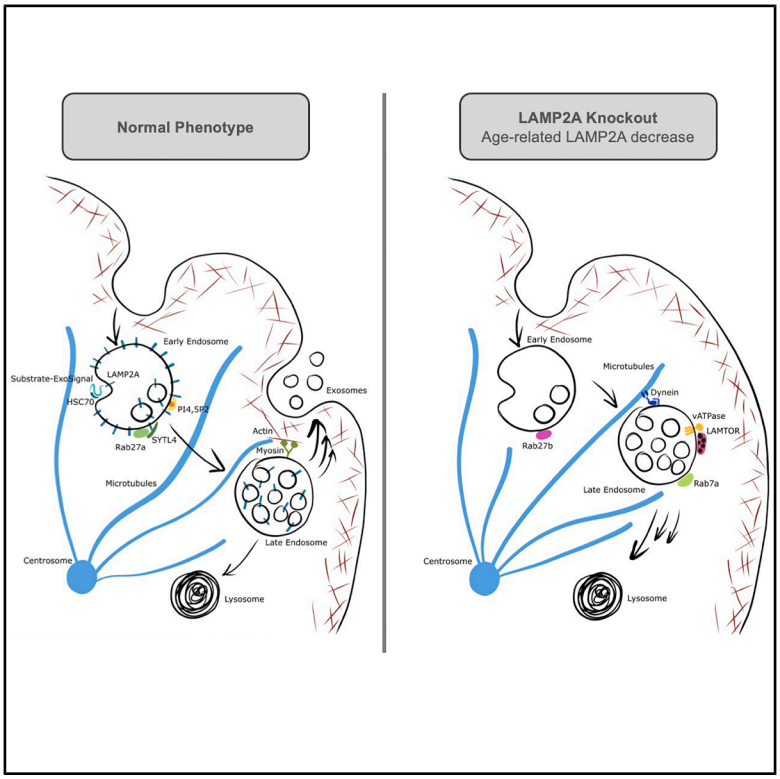

Highlights

- LAMP2A influences endosomal identity in addition to ExoSignal cargo loading
- LAMP2A KO changes Rab proteins, actin association, PI dynamics, and endolysosomal activity
- Age-related LAMP2A decline may reduce exosome signaling and homeostasis

Authors

Joao Vasco Ferreira, Luís Carvalho Ferraz, Ana da Rosa Soares, ..., Jose Silva Ramalho, Rune Matthiesen, Paulo Pereira

Correspondence

joao.ferreira@nms.unl.pt (J.V.F.), paulo.pereira@nms.unl.pt (P.P.)

In brief

Molecular biology; Cell biology

Ferreira et al., 2026, iScience *29*, 114305
January 16, 2026
https://doi.org/10.1016/j.isci.2025.114305

CellPress

iScience

CellPress
OPEN ACCESS

Article

LAMP2A regulates endosomal protein composition and membrane identity in exosome biogenesis

Joao Vasco Ferreira,[1,4,*] Luís Carvalho Ferraz,[1] Ana da Rosa Soares,[2] Mostafa Ejtehadifar,[1] Ana Sofia Carvalho,[1] Michael James Hall,[2] Judit Morello,[1] Hans Christian Beck,[3] Jose Silva Ramalho,[1] Rune Matthiesen,[1] and Paulo Pereira[1,*]

[1]iNOVA4Health, NOVA Medical School|Faculdade de Ciências Médicas, NMS|FCM, Universidade NOVA de Lisboa, Lisbon, Portugal
[2]GIMM, Gulbenkian Institute for Molecular Medicine, Edifício Egas Moniz, Avenida Professor Egas Moniz, Lisbon, Portugal
[3]Centre for Clinical Proteomics, Department of Clinical Biochemistry and Pharmacology, Odense University, Hospital, Odense, Denmark
[4]Lead contact
*Correspondence: joao.ferreira@nms.unl.pt (J.V.F.), paulo.pereira@nms.unl.pt (P.P.)
https://doi.org/10.1016/j.isci.2025.114305

SUMMARY

The endolysosomal system maintains cellular homeostasis through protein degradation and the release of exosomes that mediate intercellular communication. LAMP2A, a transmembrane protein, has been implicated in selective cargo loading into exosomes, or eLLoC. Here, we investigated how LAMP2A influences endosomal protein composition and function using mass spectrometry of endosomal and exosomal fractions from human retinal pigment epithelial cells. Loss of LAMP2A changed Rab GTPase distribution, reduced cortical actin association, and shifted phosphoinositide dynamics, leading to enhanced endosomal acidification and maturation. These changes extended beyond the loss of proteins containing ExoSignals, the canonical targeting motifs, suggesting that LAMP2A contributes broadly to endosomal identity. Experimental validation confirmed that LAMP2A deficiency reprograms endosomal fate toward degradation while influencing exosome composition. These findings highlight a role for LAMP2A in coordinating membrane identity, endosomal maturation, and intercellular communication through exosomes, providing insights into mechanisms that couple endosomal remodeling with cellular signaling and clearance pathways.

INTRODUCTION

The endolysosomal system consists of intracellular membranous compartments derived from the plasma membrane through endocytosis.[1,2] These compartments undergo dynamic transformation from early endosomes (EE) into late endosomes (LE) and eventually lysosomes.[3–5] During this process, vesicle trafficking from the Trans-Golgi Network (TGN) delivers crucial proteins required for endosome maturation.[6,7] In addition, endosomes form intraluminal vesicles (ILVs) by the invagination of their limiting membrane, which involves both the endosomal sorting complex required for transport (ESCRT)[8–10] and ESCRT-independent machinery mediated by alternative molecular components such as CD63, syntenin-1,[8,11–14] and ceramides.[15] These mechanisms facilitate the targeted degradation of proteins and lipids when multivesicular endosomes fuse with lysosomes, as well as the formation of exosomes when multivesicular endosomes fuse with the plasma membrane.

Our recent research revealed an ESCRT-independent mechanism, designated by *exosomal LAMP2A Loading of Cargo* (eLLoC), that sorts proteins into exosomes. LAMP2A, a transmembrane protein in the endolysosomal system, localizes to the endosomal membrane during the formation of ILVs and binds proteins containing specific peptide sequences called ExoSignals, thereby capturing them inside ILVs.[16,17] Interestingly, while observing endosomes, we found the asymmetrical distribution of LAMP2A, with some endosomes enriched in and others depleted of LAMP2A, suggesting that LAMP2A's role in cargo loading is likely limited to a distinct subset of endosomes.[16,17] On the other hand, mass spectrometry (MS) analysis of exosomes from LAMP2A knockout (KO) cells revealed that changes in exosome composition extended beyond the loss of ExoSignal-containing proteins,[16,17] indicating that the eLLoC mechanism is likely more intricate than initially estimated, involving unanticipated molecular players.

To investigate this further, we conducted MS analysis of endocytic pathway components following LAMP2A KO. We examined the protein content of exosomes and isolated EE and LE using subcellular fractionation techniques. This comprehensive approach provided spatial and temporal resolution into the role of LAMP2A in the endocytic pathway and exosome biogenesis, shedding light on the molecular mechanisms underlying eLLoC. MS of LAMP2A KO endosomes showed an increase in actin depolymerization and remodeling machinery, indicating a decreased presence of endosomes in cortical actin. The KO of LAMP2A also affected the presence of Rab GTPases, as well as of proteins associated with the Phosphatidylinositol Signaling System, particularly Phosphatidylinositol 4,5-bisphosphate

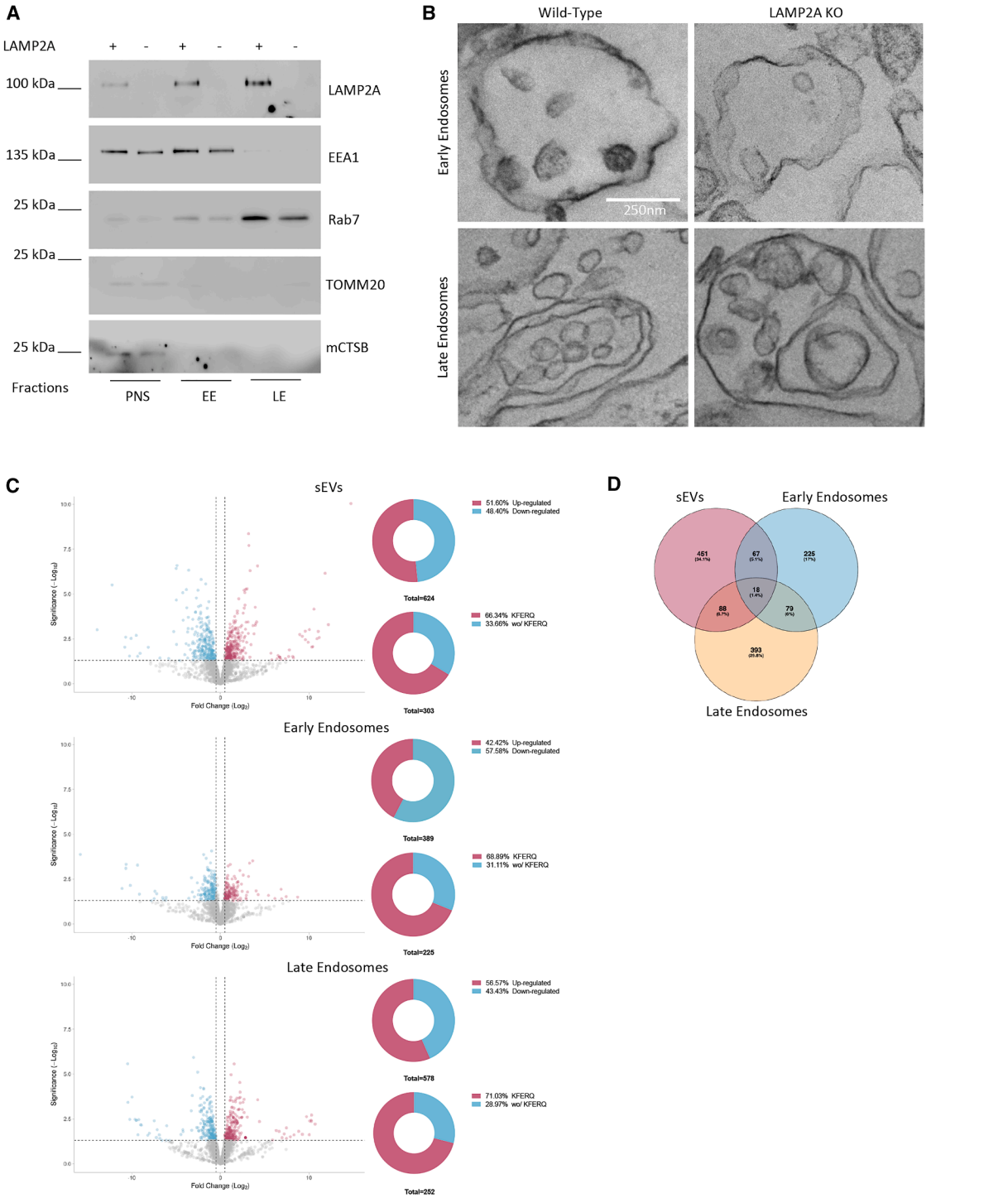

Figure 1. Proteomics data of exosome, EE, and LE fractions after LAMP2A KO, sucrose discontinuous gradients were performed as described in the protocol

(A) Post-nuclear supernatant (PNS), and EE- and LE-enriched fractions of WT and KO LAMP2A cells were loaded into an SDS-PAGE. WBs of isolated fractions were blotted with antibodies raised against the EE marker EEA1, the LE marker Rab7, the mitochondria marker TOMM20, the lysosome marker mature Cathepsin B (mCTSB), and LAMP2A.

(B) Transmission electron microscopy images of sucrose fractions from WT and LAMP2A KO cells. Scale bar set to 250 nm.

(legend continued on next page)

(PI(4,5)P2), suggesting alterations in endosomal secretion and maturation pathways. In addition, experimental validation confirmed the key findings from the MS functional analysis. These findings provide critical new details in LAMP2A's role in endosomal dynamics and its impact on exosome biogenesis and secretion mechanisms.

RESULTS

Characterization of endosomal fractions

We isolated endosomal compartments as previously described, using a discontinuous sucrose gradient.[17,18] Using this approach, it is possible to obtain two fractions, one enriched in the EE marker EEA1 and a second enriched in the LE marker Rab7 (Figure 1A). These fractions are depleted of the markers TOMM20 (mitochondria) and Cathepsin B (lysosome) (Figure 1A). When comparing both fractions using TEM, images show that Rab7 rich compartments have more ILVs inside their limiting membrane (Figure 1B), consistent with this fraction representing later endosomal compartments.

Liquid chromatography-tandem MS (LC-MS/MS) of the endosomal fractions was used to further characterize the protein contents of the fractions (Table S1). Data shows that LAMP2A isoform was identified in all fractions only in wild-type cells (SD.1). Venn diagrams representing the three biological replicates show that all fractions share over 2700 proteins amongst them, representing at least 94% of all identified proteins (SD.2). Principal component analysis reveals a low variability among samples of the same fraction, which confirms the replicates similarity. Moreover, a clear clustering of small extracellular vesicles (sEVs), EE and LE fractions along PC1 was observed, which demonstrates that each fraction has a distinct proteomic profile (SD.3). As for the LC-MS/MS of three biological replicates of exosomes, we extracted the data from *Ferreira* et al.[17], in which the exosomal fraction was extensively characterized (Table S1). Note that there is still a lack of consensus on specific markers for exosomes, and the most common method used for exosome isolation, ultracentrifugation, is unable to separate exosomes from other populations of sEVs, such as microvesicles. Following EV guidelines,[19] we were able to isolate vesicles smaller than 200 nm (including exosomes), henceforth referred to as sEVs. Among the significantly regulated proteins ($p < 0,05$) upon LAMP2A KO, in sEVs, there were 302 down-regulated and 322 up-regulated proteins, in EE 224 down-regulated and 165 up-regulated proteins, and for LE, 251 down-regulated and 327 up-regulated proteins (Figure 1C, Table S2). Some of the regulated proteins in endosomal fractions were confirmed by Western blot (SD.4). Of the down-regulated proteins, 66.34%, 68.89% and 71.03% from sEVs, EE, and LE, respectively, contained at least one ExoSignal (pentapeptide-motif)[17] (Figure 1C, Table S3). Data analysis also shows that among the regulated proteins, there are 67 common proteins between sEVs and EE, 88 between sEVs and LE, 79 between EE and LE, and only 18 were common between all compartments (Figure 1D). In addition, principal component analysis (PCA) data revealed that EE fractions and LE fractions were the most similar (SD.3A), while LE were the most affected by LAMP2A KO (SD.3B).

Functional mapping of the effects of LAMP2A KO in small extracellular vesicles and endosomal compartments associated with the endocytic pathway

To explore the functional consequences of LAMP2A KO in sEVs and endosomal compartments associated with the endocytic pathway, we conducted a detailed enrichment analysis of up-regulated and down-regulated proteins after LAMP2A KO using Gene Ontology (MF-Molecular Function, BP-Biological Process, CC-Cellular Component) and KEGG pathway databases. We considered the 10 most regulated terms of each of the databases (Figures 2A and 2B).

GO-MF analysis showed that in sEVs, the down-regulated proteins exhibited significant enrichment in PDZ domain binding (GO:0030165) (Figures 2A and 2B, 3), known to anchor membrane proteins to the cytoskeleton[20] and interact with Phosphatidylinositol 4,5-bisphosphate (PI(4,5)P2),[21] which is associated with endosome fusion to the plasma membrane.[22] In addition, down-regulated proteins in sEVs are enriched in Phosphatidylinositol binding (GO:0043325). In this regard, KEEG analysis of LE showed there was a significant enrichment in Phosphatidylinositol Signaling Proteins, in particular in proteins associated with PI(4,5)P2 (Figures 2A and 2B, 3), a further indication that there is a strong regulation of the PI(4,5)P2 after LAMP2A KO.

GO-MF analysis revealed a significant enrichment of Rab GTPases and Rab-associated proteins in sEVs (GO:0003924, GO:0017111, GO:0005092, GO:0051020) (Figures 2A and 2B, 3). Rab proteins are central regulators of vesicle formation, motility, and fusion[23] often acting in coordination with phosphatidylinositols to establish membrane identity and direct vesicle trafficking.[24–26] Among these, Rab27 isoforms show a distinct pattern upon LAMP2A KO: Rab27b is upregulated in EE, whereas Rab27a is downregulated (Figure 3). Given that Rab27b is strongly associated with exosome release,[27] this isoform switch is consistent with a shift in endosomal fate. (Figures 2B and 2C, 3). In parallel, we also observed enrichment of proteins associated with myosin binding in both EE and LE (GO:0031489, GO:0017022). Myosins are actin-based motor proteins that mediate endosomal transport and vesicle fusion events. In particular, members of the Myosin V family are well known for their role in tethering and docking endosomes at the plasma membrane[28] (Figures 2A and 2B, 3). This Rab–myosin interplay provides a mechanistic framework whereby Rab remodeling is directly coupled to cytoskeletal motors that drive vesicle positioning and exocytosis. Finally, GO-CC analysis further confirmed that sEVs are enriched in proteins associated with the actin cytoskeleton (GO:0015629, GO:0005856, GO:0005884) (Figures 2A and 2B, 3), reinforcing the view that

(C) Volcano plots of regulated proteins, using a threshold $p < 0,05$ and Log2 Fold Change of 0,5 of 3 biological replicates. Blue is for down-regulated proteins, and red is for up-regulated proteins. Pie charts show the percentage of up-regulated and down-regulated proteins in each fraction, as well as the percentage of KFERQ-containing proteins in the down-regulated ones.
(D) Venn diagram of regulated proteins after LAMP2A KO in sEVs, EE, and LE.

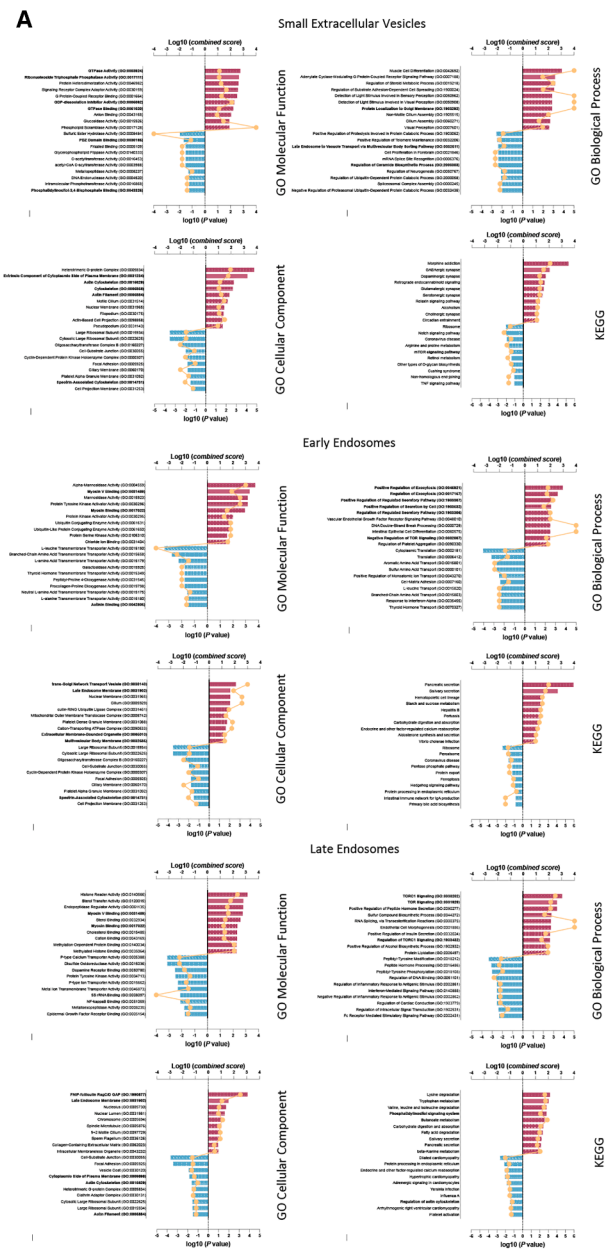

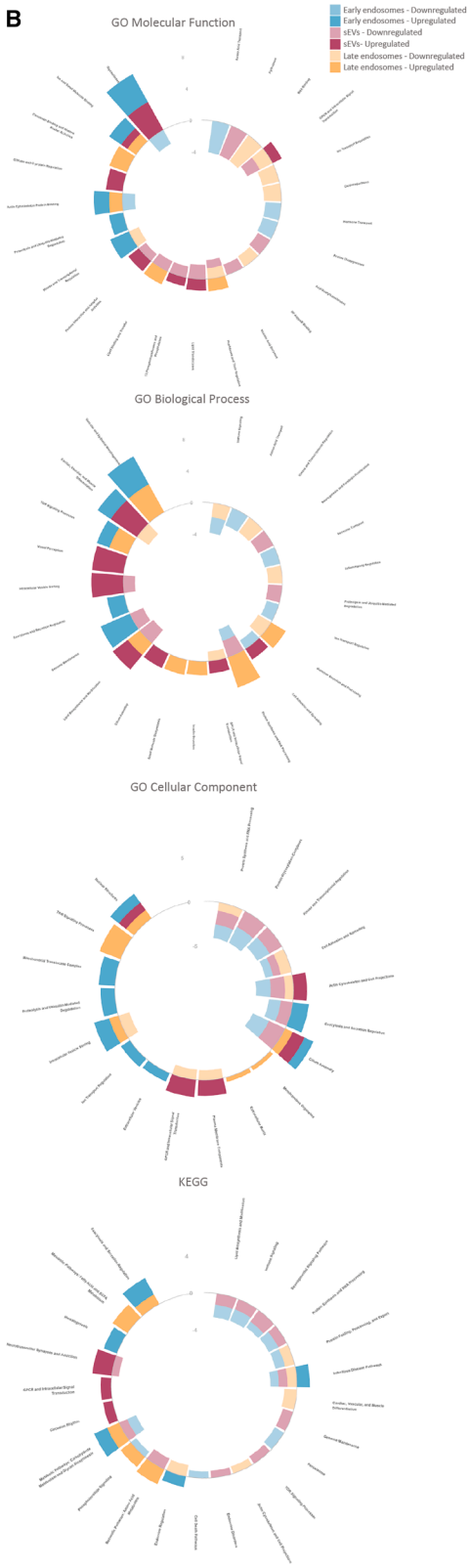

(legend on next page)

LAMP2A-dependent endosomal remodeling integrates Rab signaling, myosin function, and actin tethering to regulate vesicle dynamics.

GO-BP analysis revealed that sEVs downregulated proteins were also enriched in multivesicular body proteins (GO:0032511)[15] and regulation of ceramide biosynthetic process (GO:2000303), a lipid involved in ILVs budding at the endosomal membrane (Figures 2A–2C, 3). Regarding the up-regulated proteins, EE were enriched in numerous terms associated with exocytosis (GO:0045921, GO:0017157, GO:1903307, GO:1903532, GO:1903305) (Figures 2A–2C, 3). In addition, proteins associated with the Golgi were exclusively up-regulated in sEVs (GO:1903292), while proteins associated with TOR signaling were exclusively up-regulated in LE (GO:0038202, GO:0031929, GO:1903432) (Figures 2B and 2C, 3).

In the KEGG pathway analysis, in addition to the up-regulation of the phosphatidylinositol signaling system in LE, LAMP2A KO led to the down-regulation of proteins associated with the mTOR signaling pathway in sEVs fractions (Figures 2A–2C, 3). In LE, the down-regulated proteins were linked to the regulation of the actin cytoskeleton (Figures 2A–2C, 3).

On the other hand, GO-CC analysis shows that proteins associated with the actin cytoskeleton are up-regulated in all fractions (Figures 2A–2C, 3). Intriguingly, an alternative set of proteins associated with the regulation of the actin cytoskeleton pathway was also downregulated (Figures 2A–2C, 3).

Subsequently, we used ClueGO to analyze GO (MF, BP, and CC) and KEGG terms for large clusters in a functionally grouped network (Figure 4 and Data S5, S6, and S7). Data shows that KO of LAMP2A led to the regulation of proteins that grouped in clusters such as actin cytoskeleton (up-regulated in all fractions), Rab GTPases and phosphatidylinositides (up-regulated in sEVs and in LE), endolysosomes (up-regulated in EE and LE) and vesicle secretion (up-regulated in EE and LE and down-regulate in sEVs), and ceramides (down-regulated in sEVs), among others (Figure 4 and Data S5, S6, andS7).

Taken together, our findings show that LAMP2A depletion induces coordinated yet distinct changes across endosomal compartments and sEVs. In EE, we observe Rab remodeling (from Rab27A to Rab27B), loss of cortical actin tethering, and shifts in phosphoinositide composition that bias against exocytosis. LE display increased Rab7, v-ATPase/LAMTOR, and lysosomal enzymes, consistent with enhanced acidification and maturation. Finally, sEVs are enriched in Rab GTPases, myosin-binding proteins, and actin-associated factors, reflecting selective partitioning of membrane and cargo components. This data suggests that LAMP2A can influence endosomal identity, changing endosomal fate from secretion toward degradation, thereby linking the proteomic signatures to functional consequences along the endocytic pathway.

Experimental validation of term enrichment analysis in endosomal compartments of LAMP2A KO cells

To further confirm the functional implications of the LC-MS/MS data analysis and assess the impact of LAMP2A KO on endosomes, we isolated these subcellular compartments from wild-type, LAMP2A KO, and LAMP2A rescued cells (Figure 5A). LAMP2A rescued cells display LAMP2A localization and CD63 and EEA1 distributions indistinguishable from wild-type (SD.8 & SD.9). Western blot analysis revealed that LAMP2A KO results in a decrease in Rab27a levels, while Rab27b levels increase. This divergent change in Rab27 isoforms, initially highlighted by the LC-MS/MS data, was confirmed in our experiments. Additionally, we observed elevated levels of a number of other Rab proteins, including Rab3, Rab7, Rab8, and Rab35, consistent with our previous findings. Importantly, restoring the expression of LAMP2A in KO cells rescued the levels of all Rab proteins to wild-type levels.

Moreover, endosomal fractions from LAMP2A KO cells show a reduction in actin levels (Figure 5A). Immunoprecipitation of actin from endosome-enriched fractions further showed diminished co-precipitation with endosomes, as evidenced by reduced levels of the endosomal marker CD63 (Figure 5B). Protease-resistance assays using the trypsin incubation of isolated endosomes revealed that while EEA1 and Rab7 were partially protected, likely because they were enclosed within ILVs, actin was virtually undetected, indicating that its localization is limited to the endosomal limiting membrane (Figure 5C). Phalloidin labeling of actin filaments revealed a reduced colocalization with the endosomal markers CD63 and EEA1, a defect that was restored by LAMP2A rescue (Figure 5D and Data S10).

To assess endolysosomal acidification and Cathepsin D activity in LAMP2A KO cells, we used pH-sensitive probes (pHrodo Dextran and LysoSensor) alongside the Cathepsin D-activity dye Sir-Lysosome (Figure 5E and Data S11). LAMP2A KO increased fluorescence from both pH indicators and the Cathepsin D reporter, indicating a lower lumenal pH and elevated Cathepsin D activity. In addition, data also shows an increase in the number of acidic, enzyme-active compartments. Rescuing of LAMP2A expression restored both pH and Cathepsin D activity to wild-type levels.

To monitor cellular levels of PI(4,5)P2, we expressed a PI(4,5)P2-binding RFP fusion protein (PHΔ-RFP),[29] and for PI4P, we expressed a separate GFP-tagged probe (P4M-SidMx2-GFP).[30] We then evaluated the colocalization of these phosphoinositide probes with the endosomal marker CD63. The results demonstrated that LAMP2A KO decreases the colocalization of the PI(4,5)P2 probe while increasing the colocalization of the PI4P probe with CD63. Again, these effects were reversed by LAMP2A rescue (Figure 6).

Overall, these validation experiments indicate that LAMP2A deficiency leads to significant alterations in the endosomal Rab

Figure 2. Functional enrichment analysis of proteins from exosome, EE, and LE fractions after LAMP2A KO

(A) Top ten biological functions of the individual fraction using GO molecular function, GO biological process, and KEGG databases of 3 biological replicates. Positive values represent up-regulated terms and negative values represent down-regulated terms. Bars are transformed *p*-values, and dots are the combined score (log10(*p*-value) x *Z* score). Bold terms are the ones associated with the endocytic pathway (in GO datasets, because of redundancy, only the terms associated with the endocytic pathway and containing the largest set of proteins were considered).

(B) Circular barplots of the top 10 regulated terms for all fractions with each database using the combined score.

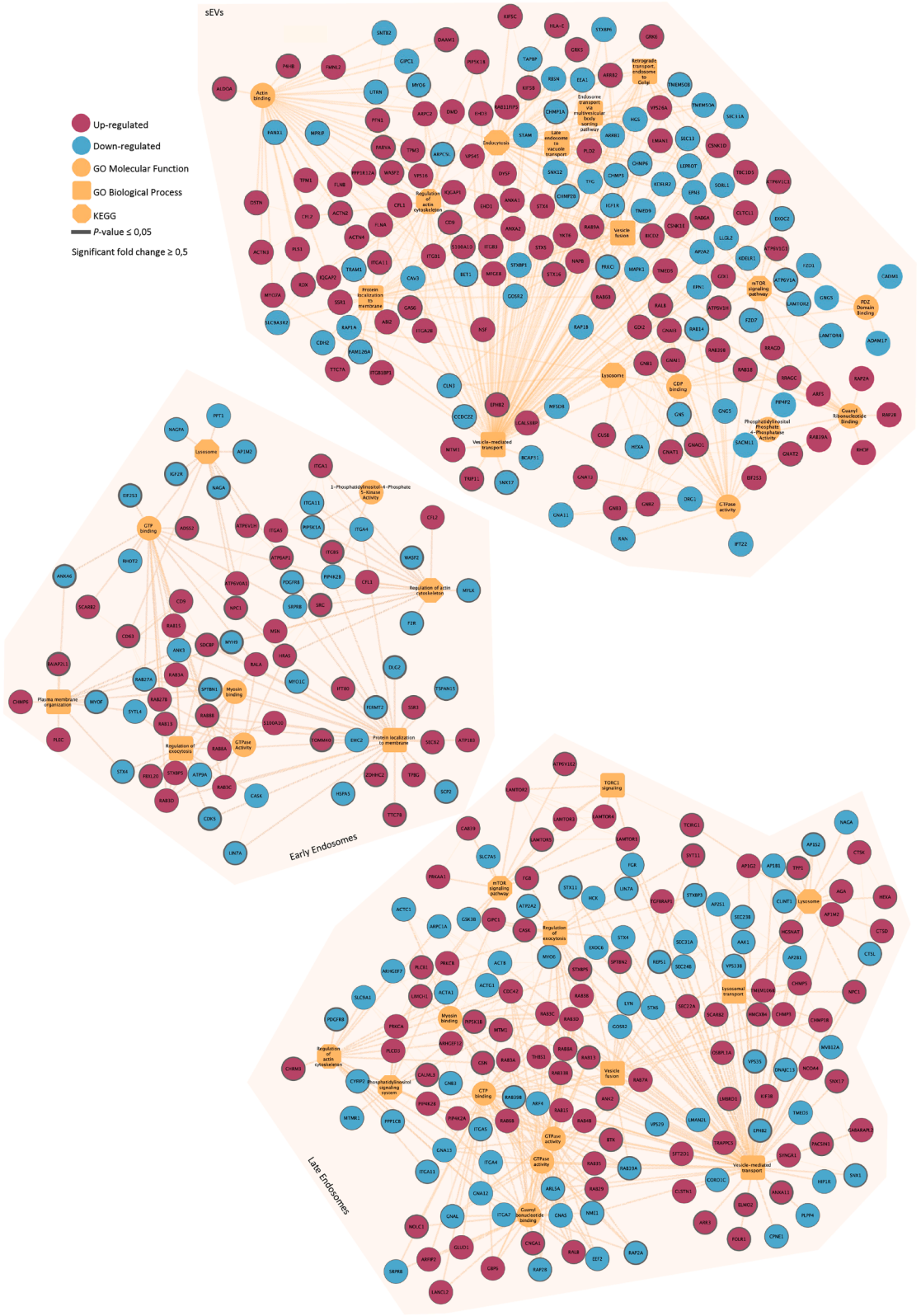

(legend on next page)

protein population and actin association, suggesting reduced endosomal association with the plasma membrane and the secretion pathway, as well as enhanced endolysosomal maturation. These findings, corroborated by changes in lysosomal acidity and phosphatidylinositol dynamics, are supported by the observations of the LC-MS/MS analysis.

DISCUSSION

In this article, we showed that the KO of LAMP2A, a single isoform of the LAMP2 protein, results in significant changes in the protein composition of endosomal compartments (Figure 7). LAMP2A has been associated with the selective degradation of proteins in the lysosome through Chaperone-Mediated Autophagy (CMA), a mechanism involving the recognition of a pentapeptide sequence biochemically related to the KFERQ-motif, which is actively present in approximately 25% of cellular proteins.[31] Recently, we also revealed that these components participate in eLLoC, facilitating the triaging and loading of proteins into exosomes.[16,17] The data herein provide evidence that LAMP2A KO further changes the protein content of endosomes, in a way that suggests a fundamental role for LAMP2A in membrane identity and endosomal maturation. It is intriguing, however, that we found a high number of proteins in exosomes that were not regulated at their compartment of origin, the LE. A possible explanation for the differences in the regulated proteins between exosomes and LE fractions is that LEs include extra limiting-membrane proteins not found in exosomes. These proteins may be asymmetrically partitioned between the endosomal membrane and ILVs during ILVs biogenesis, resulting in distinct relative-abundance profiles.

Data revealed an increase in proteins associated with the regulation of the actin cytoskeleton in both exosomes and EE after LAMP2A KO. Proteins such as Cofilin1, Cofilin2, and Destrin were upregulated upon LAMP2A KO. These proteins function by binding to actin and severing the filaments into small branches.[32,33] Conversely, in exosomes, there was a decrease in the Arp2/3 complex component ARPC2, which is necessary for the nucleation of branching actin.[34] The actin filaments surrounding endosomes have been reported to inhibit endosome maturation and retrograde movement along microtubules.[35] Additionally, actin filaments are crucial for membrane bending in endocytosis and recycling endosome tubulation.[36,37] We also observed a decrease in myosin head proteins such as MYH9 (aka non-muscle myosin heavy chain IIA heavy chain) and unconventional myosins Myo1C and Myo1E in EE upon LAMP2A KO. MyoI and MyoII play a role in the remodeling of cortical actin, displacing actin filaments around endosomes to facilitate the movement toward or away from the plasma membrane.[28] Additionally, there is a decrease in actin itself, along with proteins involved in the regulation of branched actin filaments such as CORO1C, CORO1B, ARPC1A, among others. Further experiments also revealed a significant reduction in actin levels within endosomal compartments of LAMP2A KO cells, accompanied by a decreased association between actin and endosomes. Notably, the MYO6 motor protein, which localizes to peripheral endosomes and mediates endosome association with cortical actin filaments, decreased in LE.[38] Loss of MYO6 can displace endosomes from the cell cortex and cause accumulation in the perinuclear space.[38] Therefore, our findings suggest that endosomes may be positioned farther away from the plasma membrane following LAMP2A loss.

Our results also suggest a remodeling of Rab proteins associated with endosomes after LAMP2A KO. We identified at least 41 proteins containing a RAS domain that were either upregulated or downregulated in all isolated fractions. While it is challenging to establish a definitive outcome for such a large set of proteins, some notable cases are worth mentioning. For instance, Rab27a and its effector SYTL4 were decreased in EE after LAMP2A KO, while Rab27b showed an opposite trend. Rab27 is well-known to be involved in exosome secretion, but its two isoforms, Rab27a and Rab27b, play distinct roles. Rab27a and its effector SYTL4 are essential for the docking and fusion of endosomes with the plasma membrane, while Rab27b is involved in endosome movement along microtubules.[27] Therefore, the decreased Rab27a/Rab27b ratio in EE may indicate a reduced presence of EE in the cell periphery, leading to less fusion with the plasma membrane. On the other hand, there was an increase in the presence of Rab37 and Rab39 in exosomes after LAMP2A KO, two Rab proteins recently associated with exosome secretion, providing an alternative to Rab27.[39] This suggests that LAMP2A loss might trigger compensation by recruiting additional Rab proteins capable of supporting exosome secretion. Other Rabs involved in the secretory pathway and upregulated in EE and LE include Rab3a/c/d, Rab8a/b, Rab13,[40,41] among others. Since LAMP2A KO did not significantly change exosome levels, the loss of Rab27a in endosomes, accompanied by an increase in other secretory Rabs, suggests that cells can utilize different Rabs redundantly for the same exosome secretion task. However, whether this implies that Rab27a is involved in the release of ESCRT-independent and eLLoC-associated exosomes, while other secretory Rabs preferentially associate with ESCRT-dependent exosomes, remains unclear. Furthermore, Rab7a, a Rab protein mainly localizing to LE and regulating the maturation of EE into LE,[42] was increased in LE upon LAMP2A KO. This observation indicates that LAMP2A KO may accelerate the maturation of some EE into LE or lysosomes. Rab7 is involved in v-ATPase assembly, which contributes to the acidification of LE/lysosomes and the activation of lysosomal enzymes.[43] Components of the v-ATPase were increased in both EE and LE after LAMP2A KO. Additionally, the LAMTOR/Ragulator complex, which localizes to LE/lysosomes and senses the availability of amino acids to activate MAPK and the mTOR complex,[43] also showed increased levels in LE. The increase in

Figure 3. Protein map of regulated proteins upon LAMP2A KO in sEVs, EE, and LE

Protein map of the 3 biological replicates, using the STRING network, of GO and KEGG regulated terms associated with the endocytic pathway. The yFiles algorithm for organic clustering was used. Blue represents down-regulation and red up-regulation of the protein by a significant fold change. Node border thickness represents *p*-value, such that larger *p*-values (up to 0,05) produced thinner borders, and smaller *p*-values (closer to 0) produced thicker borders. Proteins showing an absolute fold change $\geq$0,5 were considered significant.

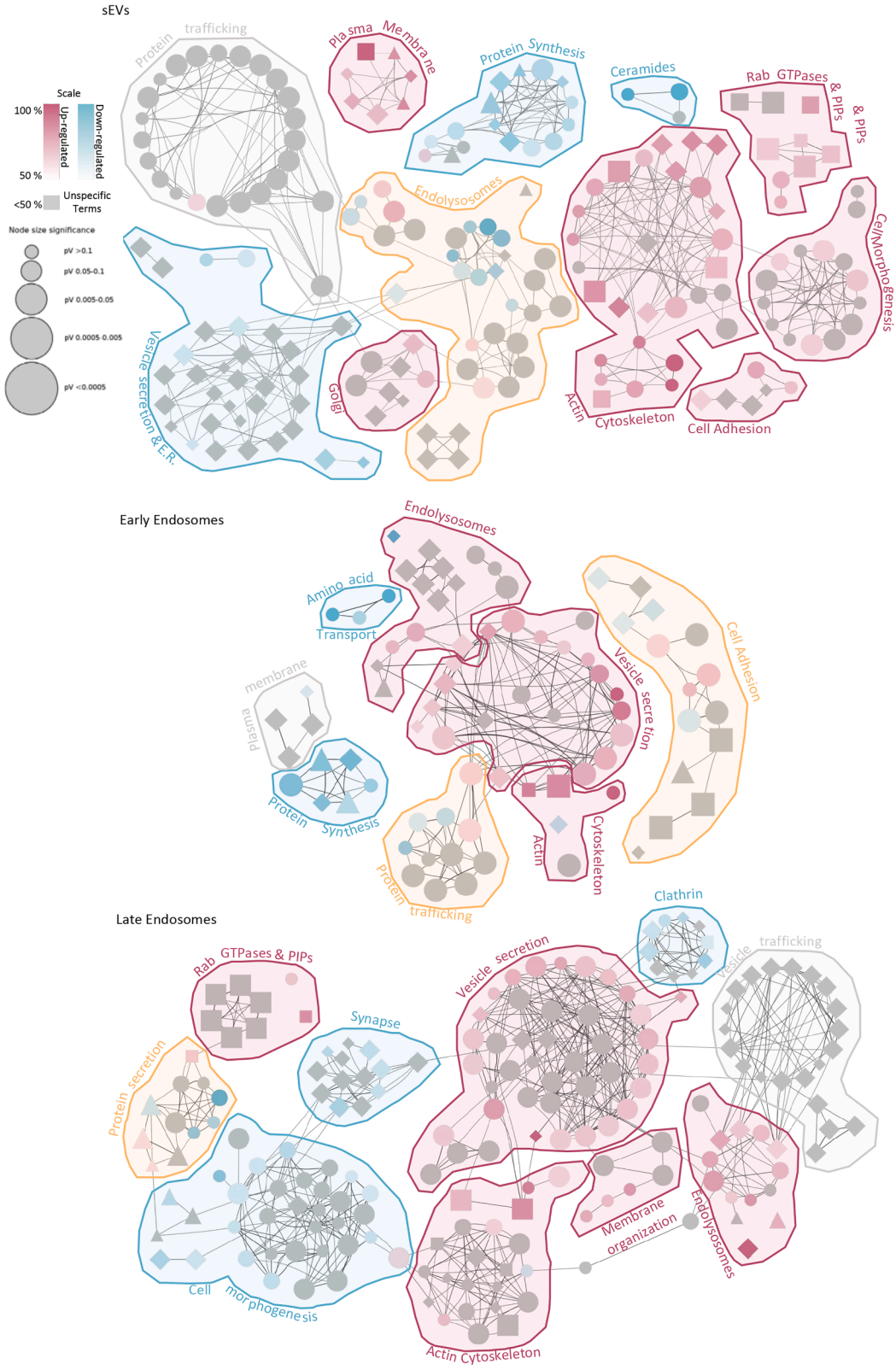

(legend on next page)

these proteins indicates that LAMP2A KO may promote the acidification of EE and enhance endosomal maturation from EE to LE. This is supported by the increase in the lysosomal enzymes CTSD and CTSK after LAMP2A KO. Our use of fluorescent probes sensitive to pH variations confirmed that LAMP2A KO leads to increased acidity and enhanced Cathepsin D activity within endolysosomal compartments.

A notable feature of endosomes after LAMP2A KO is the regulation of proteins associated with the Phosphatidylinositol Signaling System, primarily linked to PI(4,5)P2. In LE, kinases such as PIP4K2A and PIP4K2B (phosphorylating PIP5P into PI(4,5)P2),[44] as well as PIP5K1B (phosphorylating PIP4P into PI(4,5)P2)[45] were increased. Conversely, in EE, both PIP4K2B and PIP5K1A were downregulated. These changes suggest a shift toward higher levels of PI(4,5)P2 in LE and lower levels in EE after LAMP2A KO. Experiments using phosphoinositide's biosensors confirmed a reduction in PI(4,5)P2 and an increase in PI4P colocalization with endosomal markers in KO cells, highlighting a reconfiguration of endosomal phosphoinositide's composition. PI(4,5)P2 has been implicated in the fusion of autophagosomes with lysosomes for degradation.[46,47] On the other hand, PI(4,5)P2 is very abundant in the plasma membrane as well, where it is associated with endocytosis/exocytosis events by regulating actin filament remodeling, necessary for exocytosis.

Regarding membrane identity, there is a spatial and temporal coordination between Rab GTPases and phosphoinositides. For instance, PI3P to PI(3,5)P2 conversion and Rab5 to Rab7 exchange are strongly associated with the maturation from EE to LE.[24,25] While the buildup of PI(4,5)P2 in LE has not been extensively studied, it might trigger the reported fusion of endolysosomes with autophagosomes,[46,47] whereas in EE, it is likely that PI(4,5)P2 can displace Rab27a,[27] leading to reduced endosomal exocytosis and exosome secretion.

Overall, our study provides valuable insights into the effects of LAMP2A KO on the protein composition and maturation of endosomes and exosomes. The findings suggest that LAMP2A plays a crucial role in membrane identity and endosomal maturation. The regulation of proteins associated with phosphatidylinositol signaling, as well as the changes in Rab GTPases composition, suggests that LAMP2A is important in providing a specific membrane identity to endosomal compartments, with the potential to influence exosome secretion and protein degradation. One significant factor associated with aging is the decline in LAMP2A levels.[48,49] Since LAMP2A levels decrease in aging organisms, it is reasonable to anticipate that reduced LAMP2A expression could potentially impact the efficiency of eLLoC, resulting in altered protein composition within exosomes, which, in turn, may negatively influence their ability to communicate with neighboring cells and tissues. Furthermore, disruptions in endosomal functions can impact cellular clearance mechanisms, resulting in the build-up of harmful waste products, impaired protein degradation, and compromised cellular homeostasis. Targeting key players such as LAMP2A in the endolysosomal system may offer potential avenues for therapeutic interventions aimed at preserving intercellular communication and cellular homeostasis.

Limitations of the study

Proteomic approaches, while comprehensive, are subject to detection biases that may underrepresent low-abundance or transient protein interactions. Further studies in additional systems and with complementary techniques will be important to generalize these findings.

RESOURCE AVAILABILITY

Lead contact

Any additional information required to reanalyze the data reported in this article is available from the lead contact upon, João Vasco Ferreira (joao.ferreira@nms.unl.pt).

Materials availability

This study did not generate new unique reagents. All plasmids used are available from Addgene or commercial providers as listed in the key resources table.

Data and code availability

- Data. The proteomics raw and processed data generated in this study have been deposited to the PRIDE repository (ProteomeXchange Consortium: PXD070994). The dataset includes raw LC-MS/MS files and processed output tables used for downstream analysis.
- Code. No original code was generated. Analyses used publicly available software/packages as listed in the key resources table.
- Other. This article does not report any additional resources.

ACKNOWLEDGMENTS

This work was supported by the Research Unit *iNOVA4Health - Programme in Translational Medicine* (UID/4462/2025), and by the *Associated Laboratory LS4FUTURE* (LA/P/0087/2020), and by the *TransNet Project* (2022.08649.PTDC) all financially supported by Fundação para a Ciência e Tecnologia / Ministério da Educação, Ciência e Inovação. This work was also supported by the European Union, 1181 EVCA Twining Project 1182 (Horizon GA n° 101079264). We acknowledge the Metabolomics Unit of NOVA Medical School, *iNOVA4Health*, for assistance in data and analysis, in funding: *iNOVA4Health* - UID/04462 to JM. We acknowledge Michael James Hall from the Electron Microscopy Facility at the Gulbenkian Institute for Molecular Medicine for the technical expertise, sample processing and imaging. The funders had no role in study design, data collection and analysis, decision to publish, or preparation of the article.

AUTHOR CONTRIBUTIONS

J.V.F. wrote the article, prepared the figures, and designed the experiments; J.V.F., L.C.F., A.R.S., J.R., A.S.C., M.J.H., H.C.B., and J.S.R. performed the experiments. J.V.F., A.R.S., M.E., J.M., and and R.M. performed analyzed the experiments. J.V.F., A.R.S., and and P.P. conceived the initial idea of the study. All authors critically revised the article.

Figure 4. Clustering of functional groups upon LAMP2A KO

ClueGO clustering using functionally grouped networks of 3 biological replicates, with terms as nodes linked based on their kappa score (number of the common proteins between terms), where only the label of the most significant terms per cluster is shown. The node size represents the term enrichment significance. Terms with up/down-regulated proteins are shown in red/blue, respectively. The color gradient shows the up/down-regulated proportion of protein for each cluster associated with the term. Equal proportions of the two clusters are represented in gray. Approximated proportions of up and down-regulated terms are represented in orange.

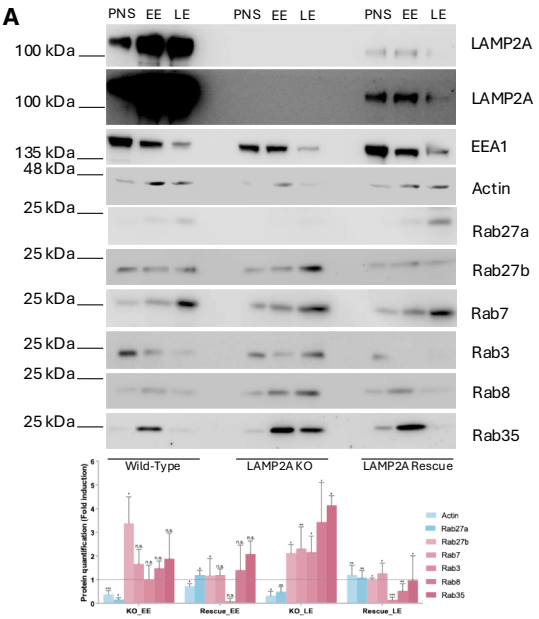

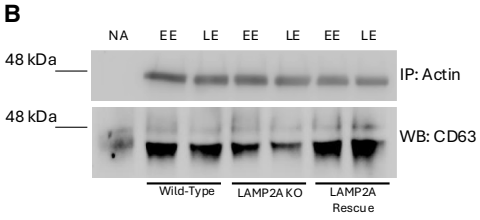

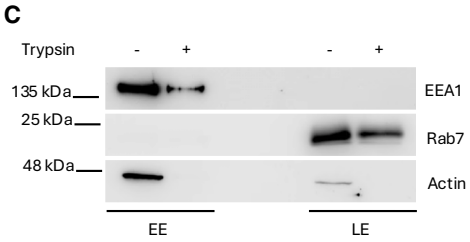

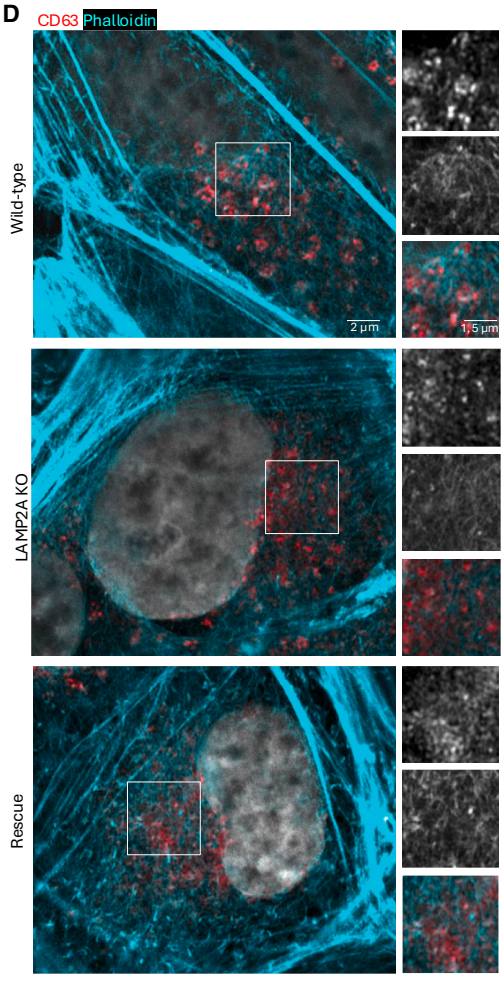

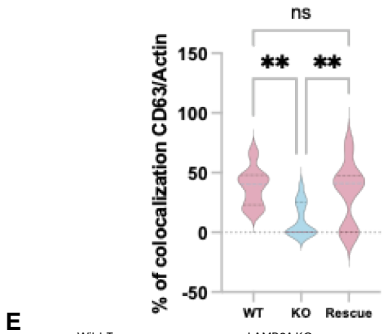

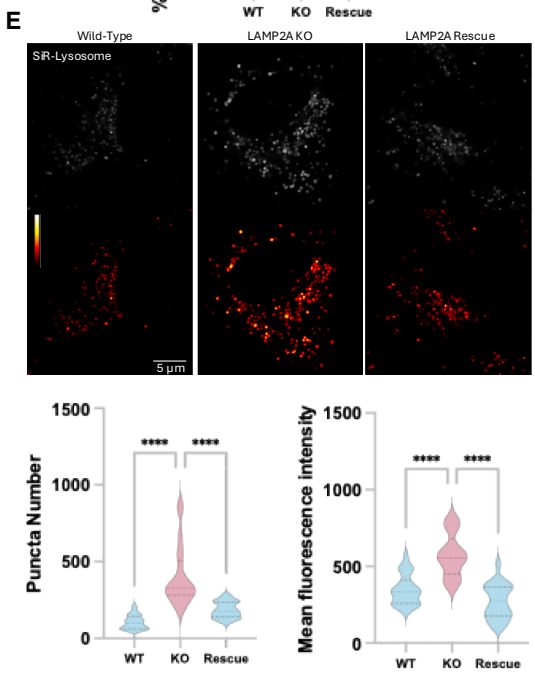

(legend on next page)

DECLARATION OF INTERESTS

The authors declare no competing interests.

STAR★METHODS

Detailed methods are provided in the online version of this paper and include the following:

- KEY RESOURCES TABLE
- EXPERIMENTAL MODEL AND SUBJECT DETAILS
  - Cell culture conditions
- METHOD DETAILS
  - Collection of EE and LE through sucrose density gradient ultracentrifugation
  - Small extracellular vesicles (sEVs) isolation
  - Endosomal immunoprecipitation
  - Antibodies and reagents
  - Transmission electron microscopy (TEM)
  - Light microscopy
  - Light microscopy image analysis
  - Preparation of peptide samples for MS analysis
  - Nano–LC-MS/MS analysis
  - MS database search
  - MS data analysis
  - Protein-protein interaction (PPI) network and functional enrichment analysis (FEA)
  - Circular barplots, volcano plots and venn diagrams
  - Lentiviral plasmids for protein expression
  - Plasmids for transfection
- QUANTIFICATION AND STATISTICAL ANALYSIS

SUPPLEMENTAL INFORMATION

Supplemental information can be found online at https://doi.org/10.1016/j.isci.2025.114305.

Received: August 1, 2025
Revised: September 11, 2025
Accepted: November 27, 2025
Published: December 2, 2025

REFERENCES

1. Skowyra, M.L., Schlesinger, P.H., Naismith, T.V., and Hanson, P.I. (2018). Triggered recruitment of ESCRT machinery promotes endolysosomal repair. Science *360*, eaar5078. https://doi.org/10.1126/science.aar5078.
2. Repnik, U., Česen, M.H., and Turk, B. (2013). The endolysosomal system in cell death and survival. Cold Spring Harb. Perspect. Biol. *5*, a008755. https://doi.org/10.1101/cshperspect.a008755.
3. Huotari, J., and Helenius, A. (2011). Endosome maturation. EMBO J. *30*, 3481–3500. https://doi.org/10.1038/emboj.2011.286.
4. Bright, N.A., Davis, L.J., and Luzio, J.P. (2016). Endolysosomes Are the Principal Intracellular Sites of Acid Hydrolase Activity. Curr. Biol. *26*, 2233–2245. https://doi.org/10.1016/j.cub.2016.06.046.
5. Klumperman, J., and Raposo, G. (2014). The complex ultrastructure of the endolysosomal system. Cold Spring Harb. Perspect. Biol. *6*, a016857. https://doi.org/10.1101/cshperspect.a016857.
6. Vergne, I., Chua, J., Lee, H.H., Lucas, M., Belisle, J., and Deretic, V. (2005). Mechanism of phagolysosome biogenesis block by viable Mycobacterium tuberculosis. Proc Natl Acad Sci USA *102*, 4033–4038. https://doi.org/10.1073/pnas.0409716102.
7. Burd, C., and Cullen, P.J. (2014). Retromer: a master conductor of endosome sorting. Cold Spring Harb. Perspect. Biol. *6*, a016774. https://doi.org/10.1101/cshperspect.a016774.
8. van Niel, G., D'Angelo, G., and Raposo, G. (2018). Shedding light on the cell biology of extracellular vesicles. Nat. Rev. Mol. Cell Biol. *19*, 213–228. https://doi.org/10.1038/nrm.2017.125.
9. Colombo, M., Raposo, G., and Théry, C. (2014). Biogenesis, secretion, and intercellular interactions of exosomes and other extracellular vesicles. Annu. Rev. Cell Dev. Biol. *30*, 255–289. https://doi.org/10.1146/annurev-cellbio-101512-122326.
10. Stuffers, S., Sem Wegner, C., Stenmark, H., and Brech, A. (2009). Multivesicular endosome biogenesis in the absence of ESCRTs. Traffic *10*, 925–937. https://doi.org/10.1111/j.1600-0854.2009.00920.x.
11. Baietti, M.F., Zhang, Z., Mortier, E., Melchior, A., Degeest, G., Geeraerts, A., Ivarsson, Y., Depoortere, F., Coomans, C., Vermeiren, E., et al. (2012). Syndecan-syntenin-ALIX regulates the biogenesis of exosomes. Nat. Cell Biol. *14*, 677–685. https://doi.org/10.1038/ncb2502.
12. Majer, O., Liu, B., Kreuk, L.S.M., Krogan, N., and Barton, G.M. (2019). UNC93B1 recruits syntenin-1 to dampen TLR7 signalling and prevent autoimmunity. Nature *575*, 366–370. https://doi.org/10.1038/s41586-019-1612-6.
13. Shimada, T., Yasuda, S., Sugiura, H., and Yamagata, K. (2019). Syntenin: PDZ Protein Regulating Signaling Pathways and Cellular Functions. Int. J. Mol. Sci. *20*, 4171. https://doi.org/10.3390/ijms20174171.
14. Roucourt, B., Meeussen, S., Bao, J., Zimmermann, P., and David, G. (2015). Heparanase activates the syndecan-syntenin-ALIX exosome pathway. Cell Res. *25*, 412–428. https://doi.org/10.1038/cr.2015.29.
15. Trajkovic, K., Hsu, C., Chiantia, S., Rajendran, L., Wenzel, D., Wieland, F., Schwille, P., Brügger, B., and Simons, M. (2008). Ceramide triggers budding of exosome vesicles into multivesicular endosomes. Science *319*, 1244–1247. https://doi.org/10.1126/science.1153124.

Figure 5. Impact of LAMP2A KO in Rab GTPases, actin binding, and endolysosomal acidity and activity

LAMP2A KO cells were transduced with lentiviral particles to express human LAMP2A.

(A) Sucrose discontinuous gradients were performed as described in the protocol. Post-nuclear supernatant (PNS), EEs and LEs enriched fractions of WT, KO LAMP2A, and LAMP2A rescue cells were loaded into an SDS-PAGE. Western blots of isolated fractions were blotted with antibodies raised against the EE marker EEA1, the LE marker Rab7, LAMP2A, Actin, Rab27a, Rab27b, Rab3, Rab8, and Rab35. LAMP2A KO leads to changes in Rab GTPases and actin composition of endosomes, which is restored by the rescue of LAMP2A expression.

(B) Immunoprecipitation of endosomal fractions using antibodies raised against actin showed that LAMP2A KO reduces the interaction of endosomes with actin, which is restored by LAMP2A rescue.

(C) Incubation of endosomal fractions with trypsin shows that while EEA1 and Rab7 are partially protected against degradation, actin is virtually undetected.

(D) Immunofluorescence using confocal microscopy of fixed cells with antibodies raised against CD63 and with phalloidin shows there is a decrease in the colocalization of LAMP2A with F-actin upon LAMP2A KO, which is recovered after LAMP2A rescue. Scale bar set to 2 μm and 1.5 μm.

(E) Cells were incubated for 2 h with a fluorescent probe that measures the activity of the lysosomal enzyme Cathepsin D (Sir-Lysosome). Confocal microscopy of the probes shows an increase in the number of puncta and of the fluorescent intensity upon LAMP2A KO, which is restored after LAMP2A rescue. The results represent the mean ± SD of at least 3 independent experiments of 15–20 cells each. Comparisons between multiple groups were performed by one-way analysis of variance (ANOVA) with Tukey's multiple comparisons tests, using GraphPad Prism 10.0 software (GraphPad Software). Scale bar set to 5 μm. (n.s. nonsignificant; *$p < 0.05$; **$p < 0.01$; ***$p < 0.001$; ****$p < 0.0001$).

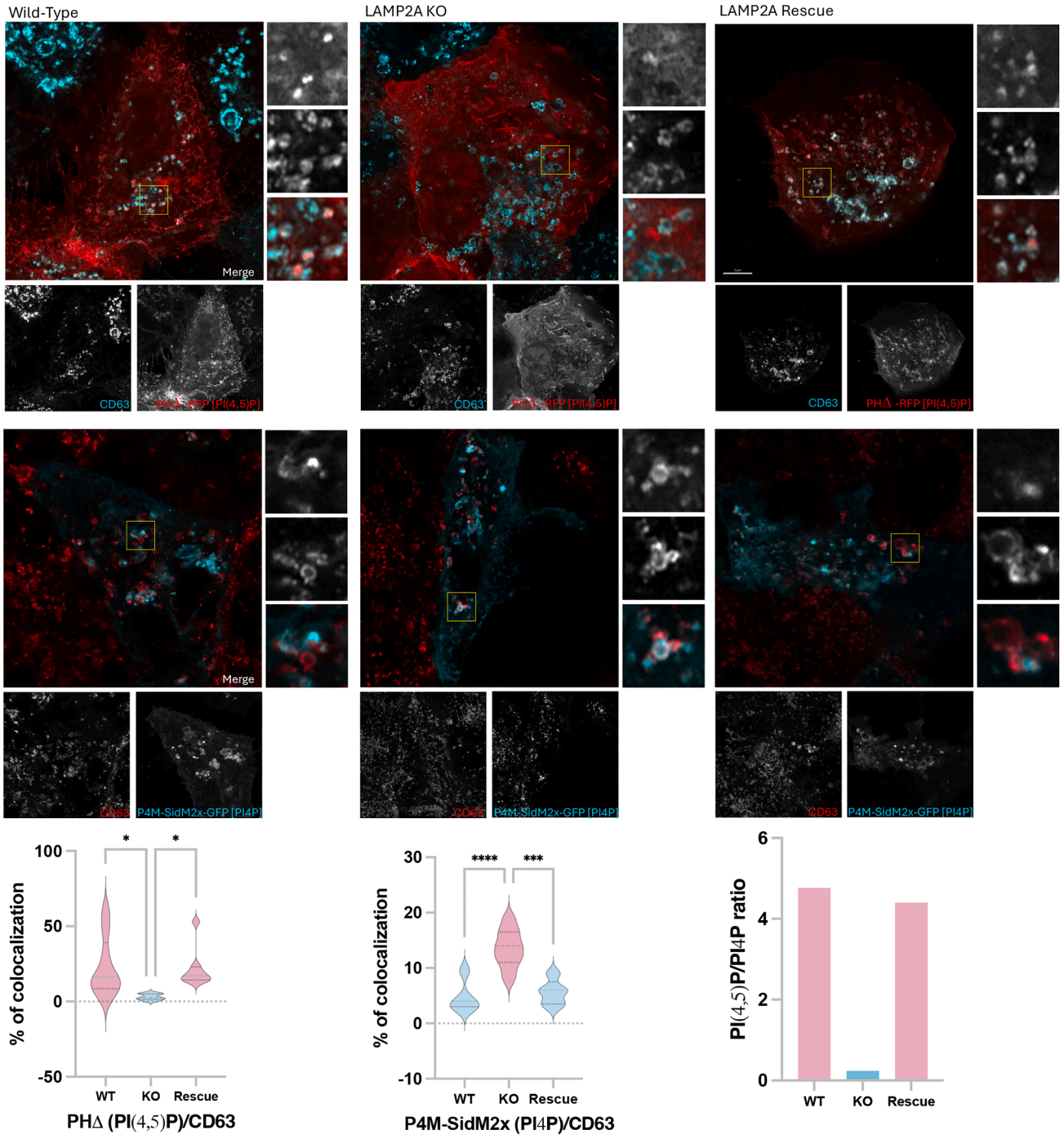

Figure 6. Effect of LAMP2A KO in the endosomal levels of PI(4,5)P and PI4P

WT, LAMP2A KO, and LAMP2A rescue cells were transfected either with PHΔ -RFP (for PI(4,5)P labeling) or P4M-SidM2x-GFP (for PI4P labeling). Immunofluorescence using confocal microscopy shows that there is an increased colocalization coefficient between PI(4,5)P and the endosomal marker CD63, while there is a decrease in colocalization coefficient between PI4P and CD63. These changes in colocalization are reversed by LAMP2A rescue. The results represent the mean ± SD of at least 3 independent experiments of 15–20 cells each. Comparisons between multiple groups were performed by one-way analysis of variance (ANOVA) with Tukey's multiple comparisons test, using GraphPad Prism 10.0 software (GraphPad Software). (n.s. nonsignificant; *$p < 0.05$; **$p < 0.01$; ***$p < 0.001$; ****$p < 0.0001$). Scale bar set to 5 μm.

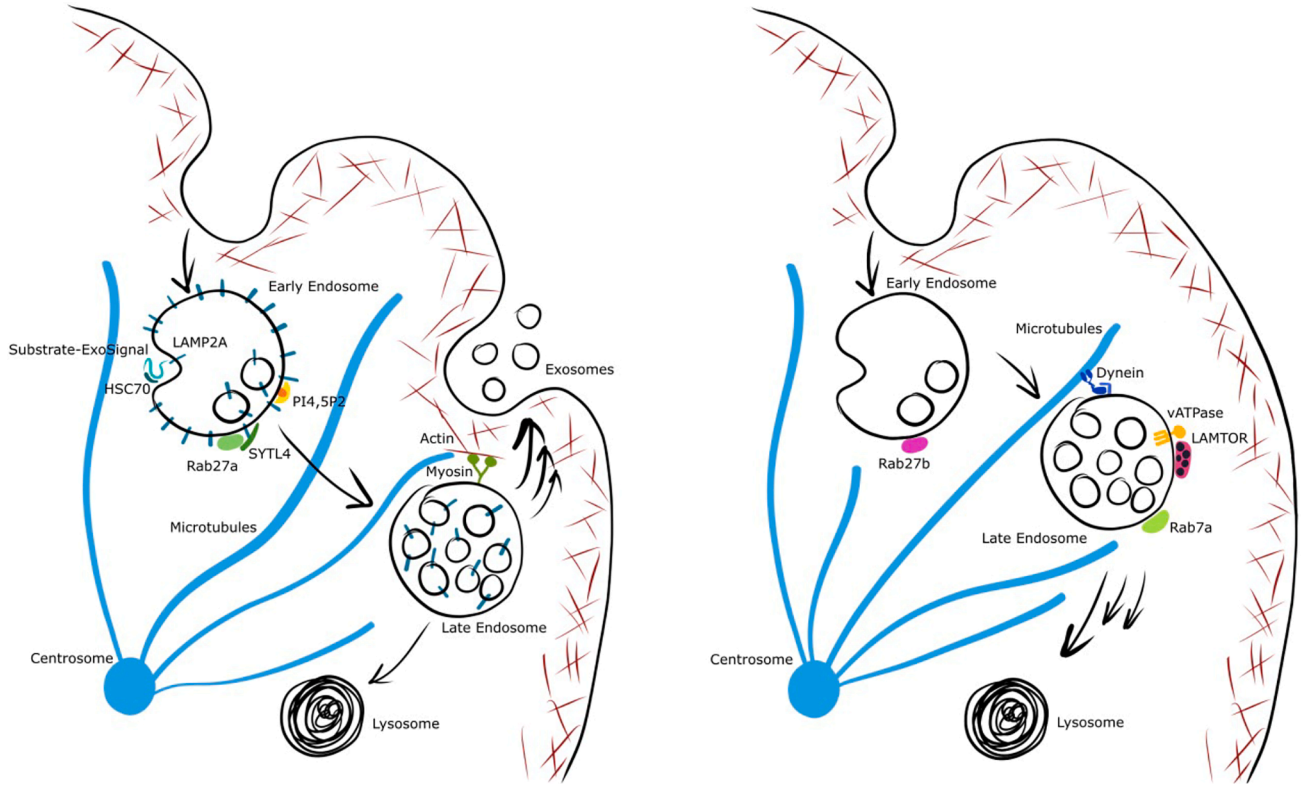

Figure 7. Schematic representation of endosomal changes induced by LAMP2A KO

Right panel: In eLLoC, a subset of endosomes recognizes cytosolic proteins containing KFERQ-like motifs through the chaperone HSC70. These proteins are targeted to the endosomal membrane, where they bind to the receptor LAMP2A. As the membrane invaginates to form ILVs, proteins remain trapped in the lumen while bound to LAMP2A. LAMP2A also facilitates the association of Rab27a and SYTL4 with the EE membrane and increases PI(4,5)P2 levels. These changes promote cortical actin association via Myosin motor proteins and subsequent fusion with the plasma membrane. Left Panel: In the absence of LAMP2A, Rab27b is recruited to the endosomal membrane instead of Rab27a, favoring microtubule binding and distancing from cortical actin. In addition, LAMP2A KO may accelerate the maturation of EE into LE or lysosomes, highlighted by an increase in proteins and complexes such as Rab7a, v-ATPase components, and the LAMTOR/Ragulator complex, indicating enhanced acidification and maturation into endolysosomes and promoting the degradative pathway.

16. Ferreira, J.V., da Rosa Soares, A., and Pereira, P. (2022). LAMP2A mediates the loading of proteins into endosomes and selects exosomal cargo. Autophagy *18*, 2263–2265. https://doi.org/10.1080/15548627.2022.2092315.

17. Ferreira, J.V., Da Rosa Soares, A., Ramalho, J., Máximo Carvalho, C., Cardoso, M.H., Pintado, P., Carvalho, A.S., Beck, H.C., Matthiesen, R., Zuzarte, M., et al. (2022). LAMP2A regulates the loading of proteins into exosomes. Sci. Adv. *8*, eabm1140. https://doi.org/10.1126/sciadv.abm1140.

18. de Araújo, M.E.G., Lamberti, G., and Huber, L.A. (2015). Isolation of early and late endosomes by density gradient centrifugation. Cold Spring Harb. Protoc. *2015*, 1013–1016. https://doi.org/10.1101/pdb.prot083444.

19. Welsh, J.A., Goberdhan, D.C.I., O'Driscoll, L., Buzas, E.I., Blenkiron, C., Bussolati, B., Cai, H., Di Vizio, D., Driedonks, T.A.P., Erdbrügger, U., et al. (2024). Minimal information for studies of extracellular vesicles (MISEV2023): From basic to advanced approaches. J. Extracell. Vesicles *13*, e12404. https://doi.org/10.1002/jev2.12404.

20. Lajoie, P., Goetz, J.G., Dennis, J.W., and Nabi, I.R. (2009). Lattices, rafts, and scaffolds: domain regulation of receptor signaling at the plasma membrane. J. Cell Biol. *185*, 381–385. https://doi.org/10.1083/jcb.200811059.

21. Egea-Jimenez, A.L., Gallardo, R., Garcia-Pino, A., Ivarsson, Y., Wawrzyniak, A.M., Kashyap, R., Loris, R., Schymkowitz, J., Rousseau, F., and Zimmermann, P. (2016). Frizzled 7 and PIP2 binding by syntenin PDZ2 domain supports Frizzled 7 trafficking and signalling. Nat. Commun. *7*, 12101. https://doi.org/10.1038/ncomms12101.

22. Kanemaru, K., Shimozawa, M., Kitamata, M., Furuishi, R., Kayano, H., Sukawa, Y., Chiba, Y., Fukuyama, T., Hasegawa, J., Nakanishi, H., et al. (2022). Plasma membrane phosphatidylinositol (4,5)-bisphosphate is critical for determination of epithelial characteristics. Nat. Commun. *13*, 2347. https://doi.org/10.1038/s41467-022-30061-9.

23. Barr, F.A. (2013). Review series: Rab GTPases and membrane identity: causal or inconsequential? J. Cell Biol. *202*, 191–199. https://doi.org/10.1083/jcb.201306010.

24. Jean, S., and Kiger, A.A. (2012). Coordination between RAB GTPase and phosphoinositide regulation and functions. Nat. Rev. Mol. Cell Biol. *13*, 463–470. https://doi.org/10.1038/nrm3379.

25. Casanova, J.E., and Winckler, B. (2017). A new Rab7 effector controls phosphoinositide conversion in endosome maturation. J. Cell Biol. *216*, 2995–2997. https://doi.org/10.1083/jcb.201709034.

26. Meng, W., Sawasdikosol, S., Burakoff, S.J., and Eck, M.J. (1999). Structure of the amino-terminal domain of Cbl complexed to its binding site on ZAP-70 kinase. Nature *398*, 84–90. https://doi.org/10.1038/18050.

27. Ostrowski, M., Carmo, N.B., Krumeich, S., Fanget, I., Raposo, G., Savina, A., Moita, C.F., Schauer, K., Hume, A.N., Freitas, R.P., et al. (2010). Rab27a and Rab27b control different steps of the exosome secretion pathway. Nat. Cell Biol. *12*, 19–30. https://doi.org/10.1038/ncb2000.

28. Miklavc, P., and Frick, M. (2020). Actin and Myosin in Non-Neuronal Exocytosis. Cells *9*, 1455. https://doi.org/10.3390/cells9061455.

29. Hammond, G.R.V., Machner, M.P., and Balla, T. (2014). A novel probe for phosphatidylinositol 4-phosphate reveals multiple pools beyond the Golgi. J. Cell Biol. *205*, 113–126. https://doi.org/10.1083/jcb.201312072.

30. Stauffer, T.P., Ahn, S., and Meyer, T. (1998). Receptor-induced transient reduction in plasma membrane PtdIns(4,5)P2 concentration monitored in living cells. Curr. Biol. *8*, 343–346. https://doi.org/10.1016/s0960-9822(98)70135-6.

31. Chiang, H.L., and Dice, J.F. (1988). Peptide sequences that target proteins for enhanced degradation during serum withdrawal. J. Biol. Chem. *263*, 6797–6805.

32. Pavlov, D., Muhlrad, A., Cooper, J., Wear, M., and Reisler, E. (2007). Actin filament severing by cofilin. J. Mol. Biol. *365*, 1350–1358. https://doi.org/10.1016/j.jmb.2006.10.102.

33. Sechi, A.S., and Wehland, J. (2004). ENA/VASP proteins: multifunctional regulators of actin cytoskeleton dynamics. Front. Biosci. *9*, 1294–1310. https://doi.org/10.2741/1324.

34. Suarez, C., Roland, J., Boujemaa-Paterski, R., Kang, H., McCullough, B.R., Reymann, A.C., Guérin, C., Martiel, J.L., De la Cruz, E.M., and Blanchoin, L. (2011). Cofilin tunes the nucleotide state of actin filaments and severs at bare and decorated segment boundaries. Curr. Biol. *21*, 862–868. https://doi.org/10.1016/j.cub.2011.03.064.

35. Harrington, A.W., St Hillaire, C., Zweifel, L.S., Glebova, N.O., Philippidou, P., Halegoua, S., and Ginty, D.D. (2011). Recruitment of actin modifiers to TrkA endosomes governs retrograde NGF signaling and survival. Cell *146*, 421–434. https://doi.org/10.1016/j.cell.2011.07.008.

36. Chen, Q., and Pollard, T.D. (2013). Actin filament severing by cofilin dismantles actin patches and produces mother filaments for new patches. Curr. Biol. *23*, 1154–1162. https://doi.org/10.1016/j.cub.2013.05.005.

37. Wang, D., Ye, Z., Wei, W., Yu, J., Huang, L., Zhang, H., and Yue, J. (2021). Capping protein regulates endosomal trafficking by controlling F-actin density around endocytic vesicles and recruiting RAB5 effectors. eLife *10*, e65910. https://doi.org/10.7554/eLife.65910.

38. Masters, T.A., Tumbarello, D.A., Chibalina, M.V., and Buss, F. (2017). MYO6 Regulates Spatial Organization of Signaling Endosomes Driving AKT Activation and Actin Dynamics. Cell Rep. *19*, 2088–2101. https://doi.org/10.1016/j.celrep.2017.05.048.

39. Matsui, T., Sakamaki, Y., Nakashima, S., and Fukuda, M. (2022). Rab39 and its effector UACA regulate basolateral exosome release from polarized epithelial cells. Cell Rep. *39*, 110875. https://doi.org/10.1016/j.celrep.2022.110875.

40. Poteryaev, D., Datta, S., Ackema, K., Zerial, M., and Spang, A. (2010). Identification of the switch in early-to-late endosome transition. Cell *141*, 497–508. https://doi.org/10.1016/j.cell.2010.03.011.

41. Castillo-Badillo, J.A., Sanchez-Reyes, O.B., Alfonzo-Mendez, M.A., Romero-Avila, M.T., Reyes-Cruz, G., and Garcia-Sainz, J.A. (2015). alpha1B-adrenergic receptors differentially associate with Rab proteins during homologous and heterologous desensitization. PLoS One *10*, e0121165. https://doi.org/10.1371/journal.pone.0121165.

42. Guerra, F., and Bucci, C. (2016). Multiple Roles of the Small GTPase Rab7. Cells *5*, 34. https://doi.org/10.3390/cells5030034.

43. Zhang, C.S., Jiang, B., Li, M., Zhu, M., Peng, Y., Zhang, Y.L., Wu, Y.Q., Li, T.Y., Liang, Y., Lu, Z., et al. (2014). The lysosomal v-ATPase-Ragulator complex is a common activator for AMPK and mTORC1, acting as a switch between catabolism and anabolism. Cell Metab. *20*, 526–540. https://doi.org/10.1016/j.cmet.2014.06.014.

44. Rameh, L.E., Tolias, K.F., Duckworth, B.C., and Cantley, L.C. (1997). A new pathway for synthesis of phosphatidylinositol-4,5-bisphosphate. Nature *390*, 192–196. https://doi.org/10.1038/36621.

45. Gonzales, B., de Rocquigny, H., Beziau, A., Durand, S., Burlaud-Gaillard, J., Lefebvre, A., Krull, S., Emond, P., Brand, D., and Piver, E. (2020). Type I Phosphatidylinositol-4-Phosphate 5-Kinases alpha and gamma Play a Key Role in Targeting HIV-1 Pr55(Gag) to the Plasma Membrane. J. Virol. *94*, e0018920. https://doi.org/10.1128/JVI.00189-20.

46. Li, S., Ghosh, C., Xing, Y., and Sun, Y. (2020). Phosphatidylinositol 4,5-bisphosphate in the Control of Membrane Trafficking. Int. J. Biol. Sci. *16*, 2761–2774. https://doi.org/10.7150/ijbs.49665.

47. Moreau, K., Ravikumar, B., Puri, C., and Rubinsztein, D.C. (2012). Arf6 promotes autophagosome formation via effects on phosphatidylinositol 4,5-bisphosphate and phospholipase D. J. Cell Biol. *196*, 483–496. https://doi.org/10.1083/jcb.201110114.

48. Cuervo, A.M., and Dice, J.F. (2000). Age-related decline in chaperone-mediated autophagy. J. Biol. Chem. *275*, 31505–31513. https://doi.org/10.1074/jbc.M002102200.

49. Zhang, C., and Cuervo, A.M. (2008). Restoration of chaperone-mediated autophagy in aging liver improves cellular maintenance and hepatic function. Nat. Med. *14*, 959–965. https://doi.org/10.1038/nm.1851.

50. McShane, E., Sin, C., Zauber, H., Wells, J.N., Donnelly, N., Wang, X., Hou, J., Chen, W., Storchova, Z., Marsh, J.A., et al. (2016). Kinetic Analysis of Protein Stability Reveals Age-Dependent Degradation. Cell *167*, 803–815.e21. https://doi.org/10.1016/j.cell.2016.09.015.

51. Lasser, C., Eldh, M., and Lotvall, J. (2012). Isolation and characterization of RNA-containing exosomes. J. Vis. Exp. e3037. https://doi.org/10.3791/3037.

52. Thery, C., Amigorena, S., Raposo, G., and Clayton, A. (2006). Isolation and characterization of exosomes from cell culture supernatants and biological fluids. Curr. Protoc. Cell Biol. *3*, 3–22. https://doi.org/10.1002/0471143030.cb0322s30.

53. Abu-Remaileh, M., Wyant, G.A., Kim, C., Laqtom, N.N., Abbasi, M., Chan, S.H., Freinkman, E., and Sabatini, D.M. (2017). Lysosomal metabolomics reveals V-ATPase- and mTOR-dependent regulation of amino acid efflux from lysosomes. Science *358*, 807–813. https://doi.org/10.1126/science.aan6298.

54. Burrinha, T., Cunha, C., Hall, M.J., Lopes-da-Silva, M., Seabra, M.C., and Guimas Almeida, C. (2023). Deacidification of endolysosomes by neuronal aging drives synapse loss. Traffic *24*, 334–354. https://doi.org/10.1111/tra.12889.

55. Matthiesen, R., Prieto, G., Amorim, A., Aloria, K., Fullaondo, A., Carvalho, A.S., and Arizmendi, J.M. (2012). SIR: Deterministic protein inference from peptides assigned to MS data. J. Proteomics *75*, 4176–4183. https://doi.org/10.1016/j.jprot.2012.05.010.

56. Carvalho, A.S., Ribeiro, H., Voabil, P., Penque, D., Jensen, O.N., Molina, H., and Matthiesen, R. (2014). Global mass spectrometry and transcriptomics array based drug profiling provides novel insight into glucosamine induced endoplasmic reticulum stress. Mol. Cell. Proteomics *13*, 3294–3307. https://doi.org/10.1074/mcp.M113.034363.

57. Cox, J., and Mann, M. (2008). MaxQuant enables high peptide identification rates, individualized p.p.b.-range mass accuracies and proteome-wide protein quantification. Nat. Biotechnol. *26*, 1367–1372. https://doi.org/10.1038/nbt.1511.

58. Smyth, G.K. (2004). Linear models and empirical bayes methods for assessing differential expression in microarray experiments. Stat. Appl. Genet. Mol. Biol. *3*, Article3. https://doi.org/10.2202/1544-6115.1027.

59. Carvalho, A.S., Moraes, M.C.S., Hyun Na, C., Fierro-Monti, I., Henriques, A., Zahedi, S., Bodo, C., Tranfield, E.M., Sousa, A.L., Farinho, A., et al. (2020). Is the Proteome of Bronchoalveolar Lavage Extracellular Vesicles a Marker of Advanced Lung Cancer? Cancers (Basel) *12*, 3450. https://doi.org/10.3390/cancers12113450.

60. Hackenberg, M., and Matthiesen, R. (2008). Annotation-Modules: a tool for finding significant combinations of multisource annotations for gene lists. Bioinformatics *24*, 1386–1393. https://doi.org/10.1093/bioinformatics/btn178.

61. Chen, E.Y., Tan, C.M., Kou, Y., Duan, Q., Wang, Z., Meirelles, G.V., Clark, N.R., and Ma'ayan, A. (2013). Enrichr: interactive and collaborative HTML5

gene list enrichment analysis tool. BMC Bioinf. *14*, 128. https://doi.org/10.1186/1471-2105-14-128.

62. Kuleshov, M.V., Jones, M.R., Rouillard, A.D., Fernandez, N.F., Duan, Q., Wang, Z., Koplev, S., Jenkins, S.L., Jagodnik, K.M., Lachmann, A., et al. (2016). Enrichr: a comprehensive gene set enrichment analysis web server 2016 update. Nucleic Acids Res. *44*, W90–W97. https://doi.org/10.1093/nar/gkw377.

63. Xie, Z., Bailey, A., Kuleshov, M.V., Clarke, D.J.B., Evangelista, J.E., Jenkins, S.L., Lachmann, A., Wojciechowicz, M.L., Kropiwnicki, E., Jagodnik, K.M., et al. (2021). Gene Set Knowledge Discovery with Enrichr. Curr. Protoc. *1*, e90. https://doi.org/10.1002/cpz1.90.

64. Garcia-Gonzalo, F.R., Phua, S.C., Roberson, E.C., Garcia, G., 3rd, Abedin, M., Schurmans, S., Inoue, T., and Reiter, J.F. (2015). Phosphoinositides Regulate Ciliary Protein Trafficking to Modulate Hedgehog Signaling. Dev. Cell *34*, 400–409. https://doi.org/10.1016/j.devcel.2015.08.001.

STAR★METHODS

KEY RESOURCES TABLE

REAGENT or RESOURCE	SOURCE	IDENTIFIER
Anti-CD63 antibody	SICGEN	AB0047
Anti-CD63 antibody (IF)	Santa Cruz Biotechnology	MX-49.129.5
Anti-EEA1 antibody	SICGEN	AB0006-200
Anti-Rab27A antibody	SICGEN	AB0045
Anti-Rab27B antibody	SICGEN	AB0072
Anti-actin antibody	Thermo Fisher	MA1-744
Anti-Cathepsin B antibody	Santa Cruz Biotechnology	SC-6493
Anti-LAMP2A antibody	Abcam	AB125068
Anti-Rab7 antibody	SICGEN	AB0033
Anti-Rab3 antibody	SICGEN	AB10032
Anti-RPN1 antibody	Invitrogen	MA5-25710
Anti-TOMM20 antibody	Abcam	AB186734
Anti-Rab8 antibody	SICGEN	AB3176
Anti-Rab35 antibody	SICGEN	AB0198
Cy5 antibody	Abcam	AB6566
Cy3 antibody	Abcam	AB97035
HRP antibody	Bio-Rad	170–6516
Rabbit anti-goat	Bio-Rad	172–1034
Goat anti-rabbit	Bio-Rad	170–6515
Pierce BCA Protein Assay Kit	Thermo Fisher	23225
ARPE-19 cell line	ATCC	ATCC-CRL-2302
pLenti6 vector	Thermo Fisher	V49610
pMD2.G plasmid	Addgene	#12259
psPAX2 plasmid	Addgene	# 12260
GFP-P4M-SidMx2 plasmid	Gift from Garcia-Gonzalo	Addgene #51472
RFP-C1-PLCdelta-PH plasmid	Addgene	#21179
BP/LR Clonase II kit	Thermo Fisher	11789013/11791019
pHrodo Dextran probe	Thermo Fisher	P10361
LysoSensor probe	Thermo Fisher	L7535
Sir-Lysosome Cathepsin D probe	Spirochrome AG	SC012
Phalloidin (actin staining)	Thermo Fisher	A22281
Lentiviral particle production system	N/A	N/A
LC-MS/MS proteomics data	This paper and Ferreira et al. (17)	PRIDE accession PXD070994
GraphPad Prism 10.0	GraphPad Software	RRID:SCR_002798
Cytoscape 3.10.0	Cytoscape Consortium	RRID:SCR_003032
STRING app v2.0.1	STRING Consortium	RRID:SCR_005223
ClueGO v2.5.10	Bindea Lab	RRID:SCR_005748
Enrichr online tool	Ma'ayan Lab	RRID:SCR_001575
DMEM with Glutamine	Biowest	L0102
Fetal Bovine Serum	Biowest	S1810
Penicillin-Streptomycin	Gibco	15140122
Nitrocellulose Membrane	GE Healthcare	88018
ECL	GE Healthcare	RPN 1235
Epon resin	EMbed	812

EXPERIMENTAL MODEL AND SUBJECT DETAILS

Cell culture conditions

ARPE-19 human cell lines (originally derived from retinal pigment epithelium human male) were cultured in Dulbecco's modified Eagle's medium (DMEM) with glutamine (Biowest). This medium was supplemented with 10% fetal bovine serum (FBS; Biowest) and penicillin-streptomycin (100 U/ml:100 μg/mL; Gibco). Both WT and LAMP2A KO[17] cells were maintained at 37°C under 5% CO_2. We selected ARPE-19 cells because their normal chromosome number facilitates CRISPR-Cas9-mediated knockout. This choice is consistent with established practices in high-profile proteomics studies, where human retinal pigmented epithelial cell lines serve as models of human cellular processes at large.[50]

METHOD DETAILS

Collection of EE and LE through sucrose density gradient ultracentrifugation

The protocol described by Ferreira et al. was used to isolate EE and LE.[17,18] In brief, 25 × 10^6 ARPE-19 cells cultured in the previously described medium were washed with ice-cold PBS and collected in a 2-mL microcentrifuge tube using a cell scraper. Subsequently, cells were centrifuged at 300 *g* (5 min, 4°C) and the resulting cell pellet loosened by cold finger in homogenization buffer [HB; 250 mM sucrose, 3 mM imidazole (pH 7.4), 1 mM EDTA, 10 mM iodoacetamide, 2 mM phenylmethylsulfonyl fluoride (PMSF), 0.03 mM cycloheximide, and 1× cocktail inhibitor from Sigma-Aldrich]. The loosened cells were then centrifuged at 1300 *g* (10 min, 4°C), the supernatant was discarded and the pellet was gently resuspended using a wide-cut tip at three times the pellet volume of HB. The suspension was passed 10 times through a 25-gauge needle in a 1-mL syringe.

70% of the homogenate volume in HB was added to the samples and centrifuged at 1600 *g* (10 min, 4°C). The supernatant was collected and subjected to another centrifugation step under the same conditions. The Post-Nuclear Supernatant (PNS) from this second centrifugation was used for organelle isolation. 5% of its volume was centrifuged at 16,000*g* (for 10 min, 4°C), with the recovered supernatant collected for cytoplasmatic fraction, which was free of vesicles. The sucrose concentration of the remaining PNS was adjusted to 40.6% and then loaded into an ultracentrifuge tube. Subsequently, 1.5 volumes of 35% sucrose solution and 1 volume of 25% sucrose solution were sequentially overlayed, with the remain volume filled with HB. The gradient was then centrifuged using a 70.1 Ti rotor at 210,000 *g* (16 h, 4°C). The fractions were collected, with LE at 25%/HB interface and EE at 35%/25% interface. Endosomal fractions were diluted in 35 mL of HB solution and centrifuged at 100,000 *g* (1 h, 4°C) using an SW 32 Ti rotor. The organelle pellets were then resuspended in a buffer selected based on the requirements of subsequent procedures.

For proteomics and WB, the fractions were collected in PBS. For proteomics, we used three biological replicates of each fraction and condition.

Small extracellular vesicles (sEVs) isolation

sEVs fractions, which are enriched in exosomes, were collected from the previously described ARPE-19 WT and KO cell lines. Cells were cultured in sEV-depleted medium, prepared according to Lässer et al.,[51] for 48 h. The medium was then harvested, and sEVs were isolated through ultracentrifugation.[51] In breif, the collected medium was subjected to differential centrifugation while kept at 4°C. The first centrifugation was at 300 g (10 min), followed by centrifugation of the resulting supernatant at 16,500 g (20 min). The pellet from this second centrifugation was used to collect the microvesicle fraction. To remove particles larger than sEVs, the supernatant was filtered using a 0.2 μm pore membrane, after which it was centrifuged at 120,000 g (70 min) in an SW 32 Ti rotor. To remove protein contaminants, the resulting pellet was washed using PBS and centrifuged at 120,000 g (70 min) in an SW 32 Ti rotor, after which sEVs were resuspended in 50 μL PBS.

For MS experiments, an extra purification step was performed to eliminate any remaining sample contaminants using a 30% sucrose cushion (Adapted from Théry. C,[52]). 4 mL of Tris/sucrose/D2O solution was gently placed on an ultracentrifuge tube. The sEVs' pellet, resuspended in 30 mL of cold PBS, was loaded on top of the sucrose cushion. and centrifuged at 100,000g (75 min, 4°C). Approximately 3.5 mL of the Tris/sucrose/D2O cushion, which now contains the isolated sEVs, was collected using an 18-G needle syringe. This fraction was diluted in 35 mL of cold PBS and centrifuged in a new tube at 100,000g (overnight, 4°C) and later resuspended in 100 μL PBS.

Endosomal immunoprecipitation

The endosomal immunoprecipitation process was adapted from a previously described protocol.[17,53] In summary, endosomal fractions were gently resuspended in a KPBS solution (136 mM KCl, 10 mM KH2PO4, pH 7.25 adjusted with KOH). Magnetic beads were prepared by incubation with an anti-actin antibody for 1 h. Subsequently, the resuspended endosomes were incubated with these magnetic beads (1 h, 4°C). The resulting immunoprecipitates were gently washed three times with KPBS using magnetos to precipitate the beads. The samples were denatured with Laemmli buffer and boiled in a dry bath (5 min, 95°C), followed by SDS-PAGE analysis. Membranes were blocked using non-fat milk (5% diluted in TBS-T) and then probed with antibodies targeting the proteins of interest.

Antibodies and reagents

The following antibodies were used: Rabbit anti-LAMP2A, dilution of 1:500 (WB) goat anti-CTSB/cathepsin B clone S-12, dilution of 1:500 (Santa Cruz Biotechnology, SC-6493); goat anti-EEA1, dilution of 1:500 (SICGEN, AB0006-200); goat anti-Rab7 dilution of 1:500 (SICGEN, AB0033); goat anti-Rab3, dilution of 1:500 (SICGEN, AB10032), mouse anti-RPN1, (Invitrogen, MA5-25710) dilution of 1:500, mouse anti-TOMM20 (Abcam, AB186734), dilution of 1:500; anti-Actin (Thermo Fischer Scientific, MA1-744), dilution 1:1000; anti-Rab27A (SICGEN AB0045), dilution of 1:500; anti-Rab27B (SICGEN AB0072), dilution of 1:500; anti-Rab8 (SICGEN AB3176), dilution of 1:500; anti-Rab35 (SICGEN AB0198), dilution of 1:500; anti-CD63 (SICGEN AB0047), dilution 1:500; mouse anti-CD63 dilution 1:100 (IF) (Santa Cruz Biotechnology, MX-49.129.5); donkey anti-mouse Cy5 dilution of 1:250 (Abcam ab6566); donkey anti-mouse Cy3 dilution of 1:250 (Abcam ab97035); horseradish peroxidase (HRP)–conjugated secondary goat anti-mouse (Bio-Rad, 170–6516), rabbit anti-goat (Bio-Rad, 172–1034), goat anti-rabbit (Bio-Rad, 170–6515), dilution of 1:5000. The following dyes were used: 1 μM of SiR-lysosome (Spirochrome AG, SC012); 100 μg/mL of pHrodo Red dextran, 10,000 MW (Thermo Fisher Scientific, P10361); and 1 μM LysoSensor Green DND-189 (Thermo Fisher Scientific, L7535). We also used nitrocellulose membranes (GE Healthcare, 88018); ECL (GE Healthcare, RPN1235); and Pierce BCA Protein Assay Kit (Thermo Fisher Scientific, 23225).

Transmission electron microscopy (TEM)

Transmission electron microscopy (TEM) was executed as described by Burrinha et al.[54] Unless otherwise stated, all reagents and materials were purchased from Electron Microscopy Sciences. Briefly, pellets of isolated organelles were fixed using 2% paraformaldehyde, 2% glutaraldehyde in 0.1 M sodium phosphate buffer (2 h, room temperature (RT)). Pellets were post-fixed with 1% osmium tetroxide and 1.5% potassium ferrocyanide (1.5 h, on ice) and then incubated with 1% tannic acid (30 min, RT). Samples were dehydrated using a series of increasing concentrations of ethanol (70%, 90%, 2 × 100%) and infiltrated/embedded with Epon resin (EMbed 812). After polymerizing the resin at 65°C overnight, the embedded pellets were sectioned at 80 nm thickness using a Reichart Ultracut S ultramicrotome (Leica) and a diamond knife (Diatome), with the resulting sections collected on copper mesh grids. Finally, these were post-stained with a solution of 2% uranyl acetate diluted in 70% methanol, followed by Reynold's lead citrate, and imaged using a Hitachi H-7650 TEM equipped with an AMT XR41 M digital camera.

Light microscopy

Cells were grown in ibiTreat 8 well slides (ibidi, 80806) and either imaged by live-microscopy or fixed with 4% PFA (w/v) in PBS for 5 min at 37°C and subsequently permeabilized with 0.05% saponin in PBS for 5 min at RT. In the latter, cells were washed with cold PBS and incubated with the primary antibodies diluted in PBS with 5% (v/v) FBS and 0.1% (w/v) BSA (20 min, RT). The cells were then washed once again and incubated with the secondary fluorochrome-conjugated antibodies diluted in the same solution as used in the primary incubation (20 min, RT). The tagged cells were analyzed using a Zeiss LSM980 Airyscan confocal microscope with an x63 oil-immersion objective.

Light microscopy image analysis

Cells were randomly imaged from to 3–4 independent biological replicates and from multiple non-overlapping fields per replicate. Image analyses were performed in randomly selected cells per micrograph/image for a total of 15–20 cells per biological replicate. For particle analysis, confocal micrographs were duplicated twice, and each copy was smoothed with a Gaussian blur ($\sigma = 1$ and $\sigma = 2$). The $\sigma = 2$ image was subtracted from the $\sigma = 1$ image to sharpen the punctate structures. A default ImageJ threshold (460–65 535) was then applied to the subtraction result, and Analyze Particles was used to extract area and mean intensity for each granule. All processing parameters (σ values, threshold limits, measurement settings) were kept constant across experiments.

Colocalization was quantified on images acquired with a confocal microscope LSM Airyscan 980 under identical settings by applying ImageJ's Colocalization Threshold tool to determine the percentage overlap between the two channels.

Preparation of peptide samples for MS analysis

The different fraction protein solutions containing SDS and dithiothreitol (DTT) were washed with 8 M urea in HEPES buffer using filtering columns. DTT and iodoacetamide were used to reduce and alkylate the proteins, respectively. Protein digestion was performed using trypsin sequencing grade (Promega) overnight.

Nano–LC-MS/MS analysis

Peptide analysis was conducted using a nano-liquid chromatography (nano-LC) system, specifically a Dionex RSLCnano 3000, which was coupled to a Q-Exactive Orbitrap mass spectrometer from Thermo Scientific.

For each analysis, a 5 μL sample was loaded onto a custom-made fused capillary pre-column (2 cm length, 360 μm outer diameter, 75 μm inner diameter). This loading step was performed at a flow rate of 5 μL per minute for 7 min. The trapped peptides were then separated on a custom-made analytical column (15–20 cm length, 360 μm outer diameter, 75 μm inner diameter) that was packed in-house with ReproSil-Pur 120 C18-AQ 1.9 μm beads. An alternative packing material mentioned was ReproSil-Pur C18 3-μm resin. Both resins were sourced from Dr. Maisch GmbH.

The separation was achieved using a binary solvent gradient at a flow rate of 300 nL per minute (nL/min). The gradient started with a 93-min linear ramp from 92% solvent A (0.1% formic acid in water) to 28% solvent B (0.1% formic acid in 100% acetonitrile), followed by a 20-min ramp from 28% to 35% solvent B. All mass spectra were acquired in positive ion mode.

Full MS scans were acquired in the Orbitrap over a mass range of 400–1200 m/z with a target value of 1,000,000 ions and a resolution of 70,000 (at m/z 200). A data-dependent acquisition (DDA) method was used to select the top 15 most intense precursor ions for fragmentation via higher-energy collisional dissociation (HCD) with normalized collision energy of 31 eV. The ion selection threshold was 25,000 counts. Maximum injection times were set to 100 ms for MS scans and 300–500 ms for MS/MS scans. Dynamic exclusion was enabled for 45 s to prevent repeated sequencing of the same ions.

MS database search

The obtained data from the 36 LC-MS runs (WT sEVs, $n = 3$, WT EE, $n = 3$, WT LE, $n = 3$, LAMP2A KO sEVs, $n = 3$, LAMP2A KO EE, $n = 3$, LAMP2A KO LE, $n = 3$; all injections were performed in duplicate) were searched using VEMS[55,56] and MaxQuant.[57] MS data was searched against the proteome database from UniProt (3AUP000005640), including common contaminants. Up to four miss cleavages were allowed. Cysteine carbamidomethylation was set as a fixed modification. Methionine oxidation; N-terminal protein acetylation; lysine acetylation; lysine diglycine; and S, T, and Y phosphorylation were set as variable modifications; mass accuracy of 10 parts per million was specified for precursor ions and 0.01 *m/z* for fragment ions. A false discovery rate (FDR) of 1% was applied at both the peptide and protein identification levels. For the VEMS search, no minimum peptide length was required. Following identification, proteins were categorized into evidence groups according to.[55]

MS data analysis

We analyzed the quantitative data files from MaxQuant and VEMS using the R statistical programming language. The protein intensity values, derived from both iBAQ (intensity-based absolute quantification) and spectral counts, were processed for further analysis. First, we removed common mass spectrometry contaminants. Following this clean up step, the data underwent a $\log_2(x+1)$ transformation and quantile normalization to standardize the distributions across samples. Statistical differences between wild-type and KO fractions were calculated by using the R package limma.[58] Correction for multiple testing was applied using the Benjamini-Hochberg method. Comparison of EV markers and potential contaminants in the current study with those in a previous study was performed as previously described.[59] Functional enrichment analyses were performed with the differentially expressed proteins and 4 different libraries: Kyoto Encyclopedia of Genes and Genomes, Gene Ontology Molecular Function and Gene Ontology Biological Process, and Gene Ontology cellular component. The significance of the enrichments were calculated by using the hypergeometric probability test as previously described.[60] For the search of KFERQ-like motifs, we used the online tool KFERQ finder (https://rshine.einsteinmed.org/).

Protein-protein interaction (PPI) network and functional enrichment analysis (FEA)

To visualize the PPI of the enriched proteins in the most correlated terms and pathways, we used the STRING application (version 2.0.1) in Cytoscape software (version 3.10.0). We loaded all differentially expressed proteins (DEPs) into the STRING application and performed queries in the STRING database. In the PPI network, we inserted the top significant terms and pathways from the list generated by STRING to show the connections between proteins, and between proteins and their terms. To investigate the functions of the DEPs, enrichment analysis was performed using the ClueGO (version 2.5.10) application in the Cytoscape software. In addition, the assessment of DEPs by ClueGO revealed the interactions between the different clusters of terms and pathways. For FEA, we loaded the up- and down-regulated DEPs as two separate groups in the ClueGO application or in the enrichr online tool.[61–63] Then, FEA was performed by acquiring gene ontology (GO) terms, including cellular process (CP), cellular component (CC), and molecular function (MF), and KEGG pathways. The query was carried out to obtain only terms and pathways with $p < 0,05$.

Circular barplots, volcano plots and venn diagrams

Circular barplots were built with the logarithm of the combined score (combination of *p*-value of Fisher's exact test and *Z* score) of the ten most significant pathways of each group according to *p*-value ranking in R statistical environment (http://www.r-project.org/, R version 4.4.1) using the *ggplot2* package. The R script was adapted from the codes that are available in "The R graph gallery" (https://r-graph-gallery.com/). The order of the protein pathways on the circular barplot was defined by the sum of the combined scores of the pathway in all fractions up and down regulated.

We used the VolcaNoseR online tool[63] to represent fold change and *p*-value of significantly regulated proteins in a volcanoplot.

We used the Venny 2.1 online tool (https://csbg.cnb.csic.es/BioinfoGP/venny.html) to create Venn diagrams.

Lentiviral plasmids for protein expression

All lentiviral particles were produced through the co-transfection of pLenti6 and pMD 2.G (VSV-G protein), and psPAX2 (Rev and Pol proteins) into the 293STAR RDPro cell line (ATCC). After 48 h, the recombinant viral particles were harvested and the cell debris was cleared through centrifugation at 3200 *g* (10 min) before use. The sequences were synthesized and cloned into the pUC57 plasmid (GeneCust).

Human LAMP2A sequence is as follow: (5′-CAAGTTTGTACAAAAAAGCAGGCTCTCGAGCAatgGTGTGCTTCCGCCTCTTCCCGG
TTCCGGGCTCAGGGCTCGTTCTGGTCTGCCTAGTCCTGGGAGCTGTGCGGTCTTATGCATTGGAACTTAATTTGACAGATTCAGAA
AATGCCACTTGCCTTTATGCAAAATGGCAGATGAATTTCACAGTACGCTATGAAACTACAAATAAAACTTATAAAACTGTAACCATTT
CAGACCATGGCACTGTGACATATAATGGAAGCATTTGTGGGGATGATCAGAATGGTCCCAAAATAGCAGTGCAGTTCGGACCTGG
CTTTTCCTGGATTGCGAATTTTACCAAGGCAGCATCTACTTATTCAATTGACAGCGTCTCATTTTCCTACAACACTGGTGATAACACA
ACATTTCCTGATGCTGAAGATAAAGGAATTCTTACTGTTGATGAACTTTTGGCCATCAGAATTCCATTGAATGACCTTTTTAGATGCA
ATAGTTTATCAACTTTGGAAAAGAATGATGTTGTCCAACACTACTGGGATGTTCTTGTACAAGCTTTTGTCCAAAATGGCACAGTGA
GCACAAATGAGTTCCTGTGTGATAAAGACAAAACTTCAACAGTGGCACCCACCATACACACCACTGTGCCATCTCCTACTACAACA
CCTACTCCAAAGGAAAAACCAGAAGCTGGAACCTATTCAGTTAATAATGGCAATGATACTTGTCTGCTGGCTACCATGGGGCTGCA
GCTGAACATCACTCAGGATAAGGTTGCTTCAGTTATTAACATCAACCCCAATACAACTCACTCCACAGGCAGCTGCCGTTCTCACA
CTGCTCTACTTAGACTCAATAGCAGCACCATTAAGTATCTAGACTTTGTCTTTGCTGTGAAAAATGAAAACCGATTTTATCTGAAGGA
AGTGAACATCAGCATGTATTTGGTTAATGGCTCCGTTTTCAGCATTGCAAATAACAATCTCAGCTACTGGGATGCCCCCCTGGGAA
GTTCTTATATGTGCAACAAAGAGCAGACTGTTTCAGTGTCTGGAGCATTTCAGATAAATACCTTTGATCTAAGGGTTCAGCCTTTCA
ATGTGACACAAGGAAAGTATTCTACAGCTCAAGACTGCAGTGCAGATGACGACAACTTCCTTGTGCCCATAGCGGTGGGAGCTGC
CTTGGCAGGAGTACTTATTCTAGTGTTGCTGGCTTATTTTATTGGTCTCAAGCACCATCATGCTGGATATGAGCAATTTTAGGGTAC
CACCCAGCTTTCTTGTACAAAGTGGACGCGT-3′) Human LAMP2A was subcloned into the Gateway adapted vector pLenti6 (Thermo Scientific) using BP/LR Clonase II (Thermo Scientific), according to the manufacturer's instructions.

Plasmids for transfection

In this work, the following plasmids were used: GFP-P4M-SidMx2 was a gift from Garcia-Gonzalo[64] and RFP-C1-PLCdelta-PH.

QUANTIFICATION AND STATISTICAL ANALYSIS

Proteomics quantification and differential analysis were performed as described in the Methods. Quantitative proteomics data from MaxQuant and VEMS outputs were analyzed in R (v4.4.1). Differential protein abundance between wild-type and LAMP2A KO fractions was assessed using limma with empirical Bayes moderated t-tests. Multiple testing was controlled using Benjamini–Hochberg FDR; proteins with adjusted $p < 0.05$ were considered significant unless otherwise specified. Functional enrichment and network analyses were carried out in Cytoscape (3.10.0) using STRING app (2.0.1) and ClueGO (2.5.10); enrichment used right-sided hypergeometric tests with appropriate correction.

For microscopy and western blot quantifications, comparisons between multiple groups were performed by one-way analysis of variance (ANOVA) with Tukey's multiple comparisons tests, using GraphPad Prism 10.0 software (GraphPad Software). The paired *t test* was used for comparisons between two groups. In all cases, *a p-value* < 0.05 was considered significant. For western blots, data are reported as the mean ± SD of at least three independent experiments (n.s. nonsignificant; $^{*}p < 0.05$; $^{**}p < 0.01$; $^{***}p < 0.001$; $^{****}p < 0.0001$). Confocal microscopy data were analyzed at the single-cell level. Results are represented as the mean ± SD of at all cells of at least 3 independent biological replicas (15–20 cells per experiment). (n.s. nonsignificant; $^{*}p < 0.05$; $^{**}p < 0.01$; $^{***}p < 0.001$; $^{****}p < 0.0001$).